New electron spin resonance (ESR) ages from Geißenklösterle Cave: A chronological study of the Middle and early Upper Paleolithic layers

Maïlys Richard, Christophe Falguères, Helene Valladas, Bassam Ghaleb, Edwige Pons-Branchu, Norbert Mercier, Daniel Richter, Nicholas J Conard

New electron spin resonance (ESR) ages from Geißenklösterle Cave: A chronological study on Middle and Early Upper Paleolithic layers

Maïlys Richard[a,b,*], Christophe Falguères[b], Hélène Valladas[c], Bassam Ghaleb[d], Edwige Pons-Branchu[c], Norbert Mercier[a], Daniel Richter[e], Nicholas J. Conard[f,g]

[a] *Institut de Recherche sur les ArchéoMATériaux-Centre de Recherche en Physique Appliquée à l'Archéologie, Université Bordeaux-Montaigne, UMR 5060, Maison de l'Archéologie, 33607 Pessac, France*

[b] *Département « Homme et Environnement », Muséum national d'Histoire naturelle, UMR 7194, 1 rue René Panhard, 75013 Paris, France*

[c] *Laboratoire des Sciences du Climat et de l'Environnement, LSCE/IPSL, UMR 8212, CEA-CNRS-UVSQ, Université Paris-Saclay, 91198 Gif-sur-Yvette Cedex, France*

[d] *GEOTOP, Université du Québec à Montréal, CP 8888, succ. Centre-Ville, Montreal, Canada*

[e] *Department of Human Evolution, Max Planck Institute for Evolutionary Anthropology, Deutscher Platz 6, 04103 Leipzig, Germany*

[f] *Tübingen/Senckenberg Center for Human Evolution and Palaeoecology, University of Tübingen, Sigwartstraße 10, 72074 Tübingen, Germany*

[g] *Abteilung Ältere Urgeschichte und Quartärökologie, Institut für Ur- und Frühgeschichte und Archäologie des Mittelalters, University of Tübingen, Schloss Hohentübingen, 72070 Tübingen, Germany*

*Corresponding author.

E-mail address: mailys.richard@u-bordeaux-montaigne.fr (M. Richard).

Keywords: ESR dating; Middle Paleolithic; early Aurignacian; Neanderthal; *Homo sapiens*; Swabian Jura

New electron spin resonance (ESR) ages from Geißenklösterle Cave: A chronological study on Middle and Early Upper Paleolithic layers

Maïlys Richard[a,b,*], Christophe Falguères[b], Hélène Valladas[c], Bassam Ghaleb[d], Edwige Pons-Branchu[c], Norbert Mercier[a], Daniel Richter[e], Nicholas J. Conard[f,g]

[a] *Institut de Recherche sur les ArchéoMATériaux-Centre de Recherche en Physique Appliquée à l'Archéologie, Université Bordeaux-Montaigne, UMR 5060, Maison de l'Archéologie, 33607 Pessac, France*

[b] *Département « Homme et Environnement », Muséum national d'Histoire naturelle, UMR 7194, 1 rue René Panhard, 75013 Paris, France*

[c] *Laboratoire des Sciences du Climat et de l'Environnement, LSCE/IPSL, UMR 8212, CEA-CNRS-UVSQ, Université Paris-Saclay, 91198 Gif-sur-Yvette Cedex, France*

[d] *GEOTOP, Université du Québec à Montréal, CP 8888, succ. Centre-Ville, Montreal, Canada*

[e] *Department of Human Evolution, Max Planck Institute for Evolutionary Anthropology, Deutscher Platz 6, 04103 Leipzig, Germany*

[f] *Tübingen/Senckenberg Center for Human Evolution and Palaeoecology, University of Tübingen, Sigwartstraße 10, 72074 Tübingen, Germany*

[g] *Abteilung Ältere Urgeschichte und Quartärökologie, Institut für Ur- und Frühgeschichte und Archäologie des Mittelalters, University of Tübingen, Schloss Hohentübingen, 72070 Tübingen, Germany*

*Corresponding author.

E-mail address: mailys.richard@u-bordeaux-montaigne.fr (M. Richard).

Keywords: ESR dating; Middle Paleolithic; early Aurignacian; Neanderthal; *Homo sapiens*; Swabian Jura

Abstract

Geißenklösterle Cave (Germany) is one of the most important Paleolithic sites in Europe, as it is characterized by human occupation during the Middle and Early Upper Paleolithic. Aurignacian layers prior to 37–38 ka cal BP feature both musical and figurative art objects that are linked to the early arrival in Europe of *Homo sapiens*. Middle Paleolithic layers yielded lithic artifacts attributed to *Homo neanderthalensis*. Since human occupation at the site is attributed to both Neanderthals and modern humans, chronology is essential to clarify the issues of Neanderthal disappearance, modern humans expansion in Europe, and the origin of the Aurignacian in Western Europe. Electron spin resonance (ESR) dating was performed on fossil tooth enamel collected from the Middle Paleolithic layers, which are beyond the radiocarbon dating range, and from the nearly sterile 'transitional' geological horizon (GH) 17 and the lower Aurignacian deposits, to cross-check ESR ages with previous radiocarbon, thermoluminescence and ESR age results. The Middle Paleolithic layers were dated between 94 ± 10 ka (GH 21) and 55 ± 6 ka (GH 18) by ESR on tooth enamel. Mean ages for GH 17, at 46 ± 3 ka, and for the lower Aurignacian layers, at 37 ± 3 ka, are in agreement with previous dating results, thus supporting the reliability of ESR chronology for the base of the sequence where dating comparisons are not possible. These results suggest that Neanderthals occupied the site from Marine Isotope Stage (MIS) 5 to the second half of MIS 3 and confirm the antiquity of early Aurignacian deposits. The presence of an almost sterile layer that separates Middle and Upper Paleolithic occupations could be related to the abandonment of the site by Neanderthals, probably during Heinrich Stadial 5 (ca. 49–47 ka),

thus before the arrival of *H. sapiens* in the area around 42 ka cal BP. These dates for the Middle Paleolithic of the Swabian Jura represent an important contribution to the prehistory of the region, where nearly all of the excavations were conducted decades ago and prior to the development of reliable radiometric dating beyond the range of radiocarbon.

1. Introduction

1.1. Dating the end of the Middle Paleolithic and the beginning of the Upper Paleolithic

The Middle to Upper Paleolithic transition has been the subject of numerous studies and has been a topic of lively debate for the past thirty years (e.g., White, 1982; Mellars, 1999; Conard, 2006; Villa and Roebroeks, 2014). Different hypotheses have been proposed to explain the disappearance of Neanderthals (*Homo neanderthalensis*) and the arrival and expansion of anatomically modern humans (*Homo sapiens*) in Eurasia during the Late Pleistocene (e.g., Mellars, 2004; Hockett and Haws, 2005; Conard et al., 2006; Verpoorte, 2006; Müller et al., 2011; Harvati-Papatheodorou, 2013). The cultural interactions between these two species are still debated and two main hypotheses are often invoked to explain the changes observed in the technical behavior during this crucial period. The presence of 'transitional industries' from around 45 ka to 30 ka (e.g., Douka et al., 2014), or as early as 48 ka (Richter et al., 2009) across Europe has been interpreted either as the result of Neanderthals and modern humans 'cohabitation', which led to cultural exchanges (the acculturation hypothesis; e.g., Hublin et al., 1996; Mellars, 2005) or as an endogenous development attributed to Neanderthals (the multiple-species model, e.g., d'Errico et al., 1998; d'Errico, 2003; Zilhão et al., 2006). The emergence of the Aurignacian, which broadly coincides with the first known *H. sapiens* in Western Europe (Higham et al., 2011, 2012) also raises questions about the development of both figurative and musical art out of Africa (e.g., Conard, 2010, 2015). During the last twenty years, the advances in dating methods have been

crucial for the construction of hypotheses regarding the beginning of the Upper Paleolithic, particularly radiocarbon (^{14}C; e.g., Higham et al., 2009). Conard and Bolus (2003, 2008) published ^{14}C ages for Aurignacian deposits from several sites in the Swabian Jura (e.g., Hohlenstein-Stadel, Hohle Fels, Geißenklösterle). Spreading from around 42 to 30 ka cal BP, these Aurignacian layers document one of the earliest evidence of artistic behavior in Western Europe (Conard, 2003, 2009). This chronology, later confirmed and improved by Higham et al. (2012), was essential to the construction of the 'Kulturpumpe' hypothesis (Conard and Bolus, 2003). According to this hypothesis, the Swabian Jura was a key center of cultural innovations for both the Aurignacian and the Gravettian, and many of the innovations from the region subsequently spread to other parts of Europe. In the 'weak' version of the Kulturpumpe hypothesis, the Swabian Jura was one of multiple regions for producing important innovations. In the 'strong' version of the hypothesis, the region would be the original source of key innovations of the Aurignacian including, but not limited to personal ornaments with a cultural dictated, three-dimensional form, figurative art, therianthropic imagery and musical instruments (Conard and Bolus, 2003).

During the last decade, radiocarbon dating played a key role in establishing well-defined transitional, late Middle and Upper Paleolithic chronologies. Methodological improvements allowed the revision of 'late chronologies', whose ages were potentially affected by modern carbon contaminations (e.g., Higham et al., 2009; Higham, 2011; Wood et al., 2013). Simultaneously, the radiocarbon calibration curve was extended to 50 ka cal BP (Reimer et al., 2013). However, for older Middle Paleolithic deposits, the chronology is still incomplete and imprecise. This is the case at Geißenklösterle Cave, which is a key site for the study of human behavior during the Late Pleistocene. The stratigraphy contains Middle and Upper Paleolithic occupations, which are separated by an occupational hiatus (Hahn, 1988). The upper part of the stratigraphic sequence, especially the Aurignacian layers, is well dated

using radiocarbon (Conard and Bolus, 2003, 2008; Higham et al., 2012), which confirms thermoluminescence (TL) ages (Richter et al., 2000).

The present work mainly focuses on the dating of the Middle Paleolithic deposits using the ESR dating method on fossil tooth enamel, in order to provide chronological constraints for the most ancient Neanderthal occupations in this cave. Samples from the 'occupational hiatus' GH 17, located between the Middle and Upper Paleolithic layers, and from the early Aurignacian GHs 15 and 16, were also analyzed with the aim of comparing ESR ages with the published ^{14}C and TL results.

1.2. Geißenklösterle Cave

Geißenklösterle Cave is located near Blaubeuren in the Swabian Jura (Baden-Württemberg, Germany), a region of low mountains in southwest Germany (Fig. 1). The cave entrance faces the Ach Valley and opens above the river Ach, a Danube tributary. The region is famous for some of the most ancient examples of both musical and figurative art, attributed to *H. sapiens* (e.g., Hahn, 1971, 1988; Conard, 2003, 2009; Conard et al., 2009; Kind et al., 2014). Middle Paleolithic occupations, attributed to Neanderthals (Conard et al., 2012), are also numerous in the Swabian Jura. At Geißenklösterle Cave, it has been suggested that these two human species successively occupied the cave, making this site and its chronology particularly important for the debate on the origins of the Aurignacian in Western Europe (Sauvet et al., 2008; Hublin, 2012; Floss, 2017).

The stratigraphy is comprised by 22 geological horizons (GH) which are grouped in several archaeological horizons (AH), documenting Middle Paleolithic to Mesolithic occupations (Fig. 2). The AHs have been defined by stratigraphic and technocultural criteria. AH IV–VIII correspond to the Middle Paleolithic sequence of the site, while AH II represents the upper Aurignacian and AH III the lower Aurignacian deposits. The many subunits of AH I

include Mesolithic, Magdalenian and Gravettian occupations. Geological horizons have been distinguished according to sedimentology and numbered 1 to 23 (Hahn, 1988; Miller, 2015). In our study, we focused on Middle Paleolithic layers (GH 21-AH VII and GH 18-AH IV), 'transitional' GH 17 (AH IIIc, almost sterile, interpreted as an occupational hiatus) and early Aurignacian layers (GHs 15 and 16, AH III).

The Aurignacian layers (AHs II and III), rich in archaeological material, are characterized by the presence of lithic tools such as carinated and nosed endscrapers, large blades with lateral Aurignacian retouch, busked and carinated burins, as well as artifacts made of ivory, bone and antler (Fig. 3). Ornaments were also documented, such as perforated fox canines or ivory pendants in AH III and a pendant made of antler in AH II (Hahn, 1988). The discovery of flutes in AH II (Hahn, 1988), dated to around 40 ka (Higham et al., 2012), documents, together with the flutes from Hohle Fels and Vogelherd, the earliest known tradition of musical instruments (Conard et al., 2009). Ivory figurines depicting humans, mammoths, bears and bisons were also uncovered in AH II (Hahn, 1988). However, in the Middle Paleolithic layers, the density of material is significantly lower. The lithic assemblages are characterized by Levallois reduction and small numbers of side scrapers and retouched flakes (Fig. 4; Conard et al., 2006).

The faunal remains documented in the Middle Paleolithic and early Aurignacian layers are associated to a cold climate, related to a 'mammoth steppe environment' (Guthrie, 1990), as attested by the presence of reindeer (*Rangifer tarandus*), mammoth (*Mammuthus primigenius*), woolly rhino (*Coelodonta antiquitatis*) and wild horse (*Equus ferus*). Given the abundant presence of cave bear (*Ursus spelaeus*), it seems that Geißenklösterle Cave was used as a hibernation den (Münzel and Conard, 2004). The high concentration in mammoth remains is likely linked to the use of ivory by humans during the Aurignacian period, as documented by the presence of ivory points (Münzel, 2001). The density of faunal remains is

much lower in the Middle Paleolithic layers, perhaps in relation with the size of the human groups that occupied the cave. The population density and the occupation intensity would have been lower during the Middle Paleolithic than during the Aurignacian period (Münzel and Conard, 2004; Conard et al., 2012).

The exceptional archaeological sequence of Geißenklösterle was the subject of several dating studies, mainly focused on the Upper Paleolithic layers, which are of great importance with regard to the emergence and development of the Aurignacian culture. Hypotheses such as the 'Kulturpumpe' and the 'Danube corridor' (according to which the Danube Valley would have been the main migration route between Southeastern Europe and the Swabian Jura; Conard and Bolus, 2003) are based on the chronology established for the lower Aurignacian deposits at Geißenklösterle. Chronological data thus played a key role in the interpretation of human dynamics during the Late Pleistocene and radiocarbon dating was consequently widely applied to samples from Upper Palaeolithic layers. Richter et al. (2000) published TL and ESR ages obtained on burnt flints and fossil tooth, respectively. The first set of ages provided a mean TL age of 40.2 ± 1.5 ka for the lower Aurignacian of AH III, coinciding with the Hengelo Interstadial. Four ESR ages were obtained on the late Middle Paleolithic layer GH 18 (AH IV), ranging from 53 ± 7 ka to 36 ± 5 ka (mean age = 43.3 ± 4.0 ka). They suggest that the last Neanderthals occupied the site between the end of MIS 4 and the beginning of MIS 3.

A large number of ^{14}C ages were obtained on bones from several laboratories, mostly from the Aurignacian horizons (AHs II and III), synthesized in Conard and Bolus (2008). They show wide variation, ranging from around 41 to 33 ka cal BP. Only a few ^{14}C ages have been reported from the Middle Paleolithic levels, ranging from around 45 (AH VIII) to 37 ka cal BP (AH IV). It has been argued by Conard (2002) and Conard and Bolus (2003) that important variations in atmospheric ^{14}C concentration between 50 ka and 30 ka were the

cause for some of the younger radiocarbon ages, based on the data obtained in North Atlantic planktonic foraminifera (Voelker et al., 2000), Japanese varves (Kitagawa and van der Plicht, 1998) and stalagmites from the Bahamas (Beck et al., 2001). Called the 'Middle Paleolithic Dating Anomaly', this phenomenon supposedly was responsible for interpretations of Middle and Upper Paleolithic occupations overlapping in time, and thus exaggerating the 'coexistence effect' between late Neanderthals and early *H. sapiens*. Higham et al. (2012) published the calibrated data from Conard and Bolus (2008) as well as new ^{14}C determinations of ultrafiltered collagen. Their results confirmed the antiquity of the Aurignacian layers, as suggested by Richter et al. (2000), which were deposited as early as 40 ka cal BP. More specifically, Higham et al. (2012) used Bayesian modelling to date the start of the early Aurignacian between 43 and 42 ka cal BP. However, regarding the transitional horizon (GH 17) and the Middle Paleolithic layers, only a few ages have been reported. Taking into account available data for the Middle to Upper Paleolithic levels, the results indicate that the early Aurignacian deposits and the almost sterile GH 17 are older than 40 ka cal BP, and the Middle Paleolithic layers range between around 52 ka cal BP (AH VII) and 35 ka cal BP (AH IV; Conard and Bolus, 2003, 2008; Higham et al., 2012).

2. Materials and methods

2.1. Sampling and sample preparation

Herbivore tooth samples (n = 13) were collected during several excavation campaigns, between 1978 and 2002 (Table 1; Supplementary Online Material [SOM] Fig. S1). The sediment matrix that embedded the teeth was therefore not preserved for radioelement analysis. Thus, a sediment sample from each dated unit—except GH 16, which had been entirely excavated—was collected on site in 2013 (Fig. 5).

The enamel, dentine and cement (in the case of equid teeth) were separated mechanically and cleaned with an electric drill. At least 30 to 40 µm was removed from each side of the enamel to exclude the volume irradiated by alpha particles contained in sediment, cement or dentine. After grinding, the enamel was sieved and the 100–200 µm granulometric fraction was used for ESR measurements. For powder samples weighing less than 500 mg, the 0–100 and 100–200 µm granulometric fractions were combined.

2.2. ESR analyses

The enamel fraction of each sample was split into six to ten aliquots depending on the amount of available starting material. One of them was kept intact (to measure the natural ESR signal) whereas the remaining five to nine aliquots were irradiated with increasing doses (40, 60, 100, 160, 250, 400, 630, 1000, 1500 Gy) using a ^{60}Co source (LABRA, CEA, Saclay, France).

The ESR analyses were performed at the Muséum national d'Histoire naturelle (MNHN, Paris, France) with an EMX Bruker ESR spectrometer working at room temperature (19 °C) with the following parameters: 5 mW microwave power, 0.1 mT modulation amplitude, 12 mT scan range, 2 min scan time and 100 kHz modulation frequency. The ESR measurements were repeated 4 times for each aliquot. The equivalent doses were calculated from the enamel T1-B2 signal at g = 2.0018 (Grün, 2000) using OriginPro 8 software (OriginLab Corporation, Northampton, USA). A mean value of ESR intensity and associated standard deviation are obtained from the four measurements and plotted as a function of the irradiation dose for the construction of the dose response curve (DRC).

The DRCs were obtained using a single saturation exponential (SSE) function (Yokoyama et al., 1985) and weighted by the inverse of the squared ESR intensity ($1/I^2$).

225 *2.3. Dose rate evaluation and age calculation*

226 The dental tissues are sampled in order to measure the ^{238}U content and isotopic ratios
227 ($^{234}U/^{238}U$ and $^{230}Th/^{234}U$) required for U uptake modelling and dose rate reconstruction. U-
228 uptake history can be reconstructed by the calculation of the U-uptake parameter, the '*p*-
229 value' (Grün et al., 1988), ranging from −1 (corresponding to an early uptake, EU) to positive
230 values (corresponding to a recent uptake, RU). For the U-series model (US; Grün et al.,
231 1988), $^{234}U/^{238}U$ and $^{230}Th/^{234}U$ values are mandatory for determining the *p*-value, while the
232 EU model does not require the computation of isotopic ratios for U-uptake modeling because
233 the *p*-value is fixed to −1. The EU model assumes that the system remained closed during
234 burial after the initial uptake of U and thus provides a minimum age based on the U-content
235 measured in the dental tissues. On the other hand, the RU model, when assuming a dose rate
236 equals to 0, provides a maximum age. Therefore, analyses are done on the enamel and on the
237 dentine and, if present, on the cement attached to the enamel. If the tooth is covered by
238 cement (e.g., *Equus*), the beta dose rate is calculated from the U-content measured in the
239 cement. For *Capra ibex* and *Rhinoceros* teeth, the external side of the enamel was in contact
240 with the sediment so the beta dose rate is calculated from ^{238}U, ^{232}Th and ^{40}K content
241 measured in the sediment.

242 U-Th analyses Dental tissues were analyzed using either inductively coupled plasma-mass
243 spectrometry (ICP-MS; n = 30) or alpha spectrometry (n = 5). U and Th isotopes were
244 extracted and purified from each dental tissue following the protocol described in Richard et
245 al. (2015). Measurements were performed using a Multi-Collector ICP-MS Nu instrument
246 (Geotop, UQAM, Montreal, Canada) following Ponte et al. (2017), or a Quadripole ICP-MS
247 Thermo Fisher Scientific Xseries II (LSCE, Gif-sur-Yvette, France) following Douville et al.
248 (2010). Alpha spectrometry measurements were performed at MNHN (Paris, France)
249 following the procedure described in Bischoff et al. (1988).

250 Sediment beta dose rate determination For equid teeth, the beta dose rate was calculated
251 considering the dentine-enamel-cement configuration, whereas for *Capra ibex* (GH 18) and
252 *Rhinoceros* (GH 21) teeth, the beta dose rate was calculated using a dentine-enamel-sediment
253 configuration (Table 1). Sediment samples (~100 g) from these units were measured at the
254 MNHN with a high-resolution, low-background Ge detector, to determine their ^{238}U, ^{232}Th,
255 and ^{40}K contents. Beta dose rates were derived from these values taking into account the
256 conversion factors of Adamiec and Aitken (1998) available in the DATA program (Grün,
257 2009).
258 In situ gamma dosimetry The gamma dose rate was measured in situ using α-Al_2O_3:C
259 dosimeters. They were inserted in the section to record the environmental dose rate as a
260 function of water content fluctuation for approximately a year (Fig. 5). A travel dosimeter was
261 used to estimate the dose recorded between the time of removal and the measurement in the
262 laboratory by these dosimeters.
263 Cosmic dose rate The cosmic dose rate in Geißenklösterle was difficult to evaluate, for two
264 reasons: the roof thickness varies from 4 to 15 m and the large entrance of the cave, opening
265 to the west, overlooks the excavation area (Figs. 5 and 6). Most of the samples were thus
266 shielded to the east, but received a cosmic contribution from the western part of the cave. It is
267 thus necessary to estimate the cosmic dose rate for each tooth sample and dosimeter according
268 its x, y and z coordinates. The cosmic dose was then modelled in 3D taking into account the
269 geometry of the cave and the varying thickness of deposits and limestone present above the
270 sample. The exposure of each sample to the cosmic rays can be modelled considering that the
271 angular repartition of the cosmic dose rate follows the $\cos^2\theta$ of the angle measured in relation
272 to the vertical axis. The contribution area of the cosmic rays can be represented as a half
273 sphere, divided into four cardinal directions (north, south, east, west). The roof thickness was
274 measured according three angles of incidence: 0°-30°, 30°-60° and 60°-90° in the four

cardinal directions (Fig. 6). The cone from 0° to 30° provides around 65% of the cosmic dose rate, while cones with angles between 30° and 60° and 60° and 90° provide around 30% and 5% of the cosmic dose rate, respectively. The cosmic dose rate was calculated according to Prescott and Hutton (1988).

ESR age calculation Ages were calculated with 1 σ error range using the DATA program (Grün, 2009). The following parameters were used for computation: an alpha efficiency of 0.13 ± 0.02 (Grün and Katzenberger-Apel, 1994) was considered; Monte-Carlo beta attenuation factors (Brennan et al., 1997) used; a water content (weight %) of 0% for the enamel and of 7 ± 5% for the dentine and cement assumed. The water content (wet weight %) in the sediment was determined by weighing the sample before and after drying in an oven for one week at 40 °C. The following values were used for individual age calculations: 15 ± 5% for GHs 15 and 16; 13 ± 5% for GH 17; 10 ± 5% for GHs 18 and 21 (7–15% measured).

3. Results

U-series analyses were conducted in order to reconstruct the U-uptake history of the dental tissues that might affect the dose rate (Table 2). U-content is low for all samples, ranging from 0.0023 to 0.3650 ppm. For samples with extremely low U and Th contents, ^{234}U and ^{230}Th signals were too weak and isotopic ratios ($^{234}U/^{238}U$, $^{230}Th/^{234}U$ and $^{230}Th/^{232}Th$) were not determined. Otherwise, $^{234}U/^{238}U$ activity ratios were superior to 1 and $^{230}Th/^{234}U$ inferior to 1, as expected. In Geißenklösterle cave, the low U-content of the teeth generates dose rates close to 1 $\mu Gy \cdot a^{-1}$ for most of the dental tissues. When isotopic ratios were determined, US-ESR ages were calculated but, as expected, were not distinguishable from the EU-ESR ages, except for sample GK 57-2609 (SOM Table S1). More specifically, this tooth has the highest U-content measured in the enamel (0.2583 ± 0.0016 ppm). Its internal (α + β) dose rate is consequently not negligible and requires the use of the US model. Considering

these observations, the ages can be calculated using the EU model, except for sample GK 57-2609, which requires a modelling of the internal dose rate using the US model.

^{238}U, ^{232}Th and ^{40}K contents measured in the sediment and used for the calculation of the beta dose rate received by the teeth sampled in GHs 18 and 21 are given in Table 3. The radioelements content is lower in GH 21 than in GH 18, while the gamma dose rates recorded by the dosimeters (Table 4) are similar (60 and 67 µGy/a, respectively). Nonetheless, we can observe that both gamma dose rate and radioelements content measured in the sediment from GHs 15, 17, 18 and 21 tend to decrease with depth (Tables 3 and 4). The mechanism that produced these results needs further investigation. No disequilibrium was observed except for the sediment from GH 15 for which a slight disequilibrium (lower than 10%) was determined.

The values recorded by the dosimeters correspond to a low radioactive environment, with gamma dose rates ranging from 60 $\mu Gy \cdot a^{-1}$ (GH 21) to 145 $\mu Gy \cdot a^{-1}$ (GH 15; Table 4). Three dosimeters were placed each in GHs 15 and 17, and for each GH a mean value with its standard deviation was calculated. However, we noticed that the gamma dose values recorded in GH 15 were scattered, from 66 to 145 $\mu Gy \cdot a^{-1}$. Since the sedimentary matrix containing the teeth has been excavated, the gamma dose rate is measured from the remaining sections. It is thus not possible to determine if the teeth belonged to the lower or the higher dosimetric environment. The mean value of 108 ± 42 $\mu Gy \cdot a^{-1}$ was thus used for the age calculation, but could be unrepresentative of the dose rate underwent by the samples unearthed from this GH (see discussion on the spatial variation of the gamma dose rate in Richter, 2007). For GH 16, which was entirely excavated, a mean value of 106 ± 23 $\mu Gy \cdot a^{-1}$ was computed from the values recorded in GHs 15 and 17. For GHs 18 and 21, only one dosimeter could be inserted in each unit, due to the collapse of the section during fieldwork.

Ages, equivalent doses and dose rates are presented in Table 5. They range from 94 ± 10 ka (base of the sequence, GH 21) to 35 ± 8 ka (top of the sequence, GH 15). Dose response

curves are available in SOM Figs. S2–S14. GK 57-2609 is the only sample for which the EU-ESR (56 ± 6 ka) and the US-ESR (73 ± 9 ka) ages are significantly different. In this specific case, the EU-ESR age represents the minimum age, and the US-ESR age is thought to be more reliable. Indeed, if we consider the U-contents measured in all the enamels, this one is the highest (≈0.26 ppm), inducing a significant internal (α + β) dose rate. *P*-values for this sample derived from the US model are 0.80 ± 0.40 for the enamel and 2.15 ± 0.17 for the dentine, describing sublinear and recent uptakes, respectively. In contrast, for all other samples, EU, LU (linear uptake, Ikeya, 1982), RU and US-ESR ages are not distinguishable, with differences lower than 6% (SOM Table S1).

Table 5 shows that equivalent doses (D_e) obtained using a SSE function (Fig. 7) are low, ranging from 5 to 12 Gy. To avoid equivalent dose overestimation, Duval and Grün (2016) recommended using a maximum irradiation dose (D_{max}) up to 10 times the D_e. Since D_{max} is 1500 Gy, D_{max}/D_e values are high, included between 131 and 302 (SOM Table S2). To test the impact of high irradiation steps on the D_e estimation, equivalent doses were calculated by removing the highest experimental points on the dose response curve for three samples whose D_e are inferior to 11 Gy. The maximum difference between the D_e is less than 3% (SOM Table S3), suggesting that high D_{max}/D_e values do not impact the determination of the D_e for the samples analyzed in this study. Moreover, for GH 18, no significant variation can be observed between D_e obtained in this study, ranging from 8.7 ± 0.2 to 10.9 ± 0.4, with those published by Richter et al. (2000), ranging from 8.1 ± 0.7 to 10 ± 0.6 Gy and obtained with exponential dose steps from 5 to 960 Gy. These low D_e values are correlated with low U-content and environmental dose rates. Indeed, gamma (plus beta, if applicable) dose rates from the sediment are very low, ranging from 64 ± 15 (GH 21) to 108 ± 42 $\mu Gy \cdot a^{-1}$ (GH 15). However, the cosmic dose rate is significant, varying from 38 to 99 $\mu Gy \cdot a^{-1}$ depending on sample location. It represents up to 47% (GK 75-426) of the dose rate. By contrast, the sum of

the dose rates from each tissue does not exceed 6%, at the exception of GK 57-2609, which rises to 13% (Fig. 8).

4. Discussion

These ESR ages obtained for the lower part of the stratigraphic sequence provide new information regarding the Middle Paleolithic occupations of the cave (Fig. 9). The two ESR results obtained for GH 21 (AH VII), of 94 ± 10 ka (GK 47-583) and 73 ± 9 ka (GK 57-2609), indicate an occupation during the MIS 5, and a weighted mean age of 82 ± 9 ka may be calculated. However, these two ages do not overlap. Two hypotheses could explain the age difference: 1) the deposition time of this layer is in the order of 10–40 ka or 2) diagenetic processes during burial could have altered GK 57-2609, which has a higher U-content (around 0.26 ppm) in the enamel than in the dentine. Indeed, enamel is less porous than dentine and cement and so the U-content is generally lower (e.g., Eggins et al., 2003; Kohn, 2008). In the case of GK 57-2609, the U-content of 0.26 ppm in the enamel is not well understood, especially if we consider the other dated samples, for which the U-content does not exceed 0.03 ppm. However, this hypothesis requires further investigation to assess the preservation state of the tooth sample. Nonetheless, if we take into account the RU-ESR age of this sample (maximum age calculated assuming a dose rate from the dental tissues equal to 0), of 83 ± 9 ka, it is in agreement with both EU-ESR and RU-ESR ages for GK 47-583 (SOM Table S1), of 94 ± 10 ka (EU) and 100 ± 12 ka (RU).

For GH 18 (AH IV), the new ESR ages, ranging from 65 ± 8 ka to 55 ± 6 ka, are somewhat older than previous ESR ages (Richter et al., 2000; from 53 ± 5 ka to 36 ± 5 ka; Fig. 10). The weighted mean age is 60 ± 4 ka, while the one published by Richter et al. (2000) is 43 ± 4 ka. The equivalent doses reported in Richter et al. (2000) for the dated teeth range from 8.1 ± 0.7 to 10 ± 0.6 Gy and are similar to those obtained in the present study, ranging

375 from 8.7 ± 0.2 to 10.9 ± 0.4 (Table 5). The beta dose rate from the sediment was calculated
376 from delayed neutron counting (U) and neutron activation (Th, K; Richter et al., 2000) and
377 ranged from 79 to 151 $\mu Gy \cdot a^{-1}$. However, our beta dose rate (measured using laboratory
378 gamma ray spectrometry) is lower, ranging from 32 ± 4 to 44 ± 6 $\mu Gy \cdot a^{-1}$. While in gamma
379 spectrometry bulk samples, which include small pebbles, rocks, bones, etc. are analyzed, the
380 small sample for NAA consisted of clayey sediment only. This was taken as a more realistic
381 scenario by Richter et al. (2000) considering the short ranged beta contribution (around 2 mm)
382 and that teeth are usually encased by clayey sediments. It could explain why the beta dose
383 rates measured by Richter et al. (2000) are much higher than those we measured using
384 laboratory gamma ray spectrometry. Moreover, cave deposits are generally heterogeneous
385 dosimetric environments, due to the presence of limestone rocks for instance. Lateral
386 variation of the gamma dose rate should be also considered as a potential source for the age
387 discrepancy. Indeed, a value of 67 $\mu Gy \cdot a^{-1}$ was measured in GH 18 for the present study,
388 while previous published ages by Richter et al. (2000) were calculated using a value of 39
389 $\mu Gy \cdot a^{-1}$.These results suggest that Neanderthals inhabited the cave not only at the beginning
390 of MIS 3 but during MIS 4 as well. These ages, obtained for the lower part of the sequence,
391 are systematically older than ^{14}C ages. Their antiquity, combined with the fact that ^{14}C ages
392 obtained previously do not increase as a function of depth, indicate an occupation time
393 beyond the limit of radiocarbon, i.e., older than 50 ka (Fig. 10). De facto, uncalibrated ^{14}C age
394 published by Higham et al. (2012) for GH 21, of 48.6 ± 3.2 ka, should be considered as a
395 minimum age. The two sets of results obtained for GHs 21 and 18 allow, for the first time, to
396 constrain Neanderthal occupation at Geißenklösterle Cave and demonstrate the antiquity of
397 the settlement in the cave, starting during MIS 5 (Fig. 9).

398 Ages derived for the transitional horizon (GH 17, AH IIIc) range from 48 ± 6 ka to 44
399 ± 5 ka, and are in agreement with ^{14}C ages (Fig. 10), except for the age published by Conard

400 and Bolus (2003). This date was not obtained using the ultrafiltration protocol, used to
401 remove modern contaminants, which could explain why it appears younger than those
402 published by Conard and Bolus (2008) and Higham et al. (2012). The fact that this unit is
403 almost sterile suggests an interruption of human activities in the cave, probably during a cold
404 phase. Indeed, the weighted mean age of this unit (46 ± 3 ka) coincides with Greenland
405 Stadial (GS) 12 or 13. Stratigraphic discontinuities between Middle and Upper Paleolithic
406 layers have also been identified elsewhere in Europe (e.g., Spain: Mallol et al., 2012; Italy:
407 Peresani, 2008). This supports the hypothesis of a regional extinction or substantial
408 depopulation of Neanderthals in the Swabian Jura prior to the arrival of modern humans
409 (Conard et al. 2006). Radiocarbon ages indicate that early Aurignacian deposits predate
410 Heinrich Stadial 4 (around 40–38 ka; Higham et al., 2012). Taking into account all available
411 chronological data, GH 17 could have been deposited during Heinrich Stadial 5, which took
412 place between ca. 49–47 ka (Svensson et al., 2008).

413 For the Aurignacian layers (GHs 15 and 16, AHs III, IIIa and IIIb), ESR ages are in
414 agreement with ^{14}C and TL data (Fig. 10). Three ages are available for GH 15, of 40 ± 10 ka,
415 38 ± 8 ka and 35 ± 8 ka but have a large error due to the large variation of the gamma dose
416 rate recorded by the dosimeters (see Table 4). A weighted mean of 37 ± 5 ka may be obtained.
417 These ages are constrained by the two other ages obtained for GH 16 (50 ± 8 ka and 34 ± 4;
418 Fig. 9), for which a weighted mean age of 37 ± 8 ka may be calculated. The difference
419 between these two ages could be explained by their stratigraphic position or by the spatial
420 variation of the in situ gamma dose rate, which cannot be directly measured in GH 16. The
421 youngest is attributed to a tooth sampled at a depth of 3.43 m, whereas the oldest age is
422 associated with a sample found at a depth of 3.70 m (Fig. 9). However, since this layer was
423 entirely excavated, the gamma dose rate cannot be measured in situ and no sediment was
424 available for laboratory gamma ray spectrometry. It was thus not possible to assess the degree

425 of heterogeneity for GH 16. Considering that the ages for this layer were computed using the
426 gamma dose rate recorded in both GHs 15 and 17, we do not exclude a local variation of the
427 gamma dose rate as observed in GH15, which would account for the age discrepancy.
428 Considering ESR ages obtained for both GHs 15 and 16, a weighted mean age of 37 ± 3 ka
429 may be obtained for the lower Aurignacian layers.
430
431 **6. Conclusions**
432 ESR dating was used to date herbivorous teeth from Middle Paleolithic and early
433 Aurignacian horizons in order to extend the chronological framework of the Geißenklösterle
434 sequence (Swabian Jura, Germany). The ESR results were compared with previous ^{14}C, ESR
435 and TL results available for the Aurignacian and the uppermost Middle Paleolithic layers.
436 They demonstrate the potential and limitations of such application in a heterogeneous
437 dosimetric environment. Indeed, the difficulty in reconstructing the gamma dose rate and
438 estimating the cosmic contribution to the annual dose induce large uncertainties in the ages
439 obtained for the early Aurignacian deposits. The agreement between TL and/or ^{14}C and ESR
440 ages obtained on GH 17 and early Aurignacian deposits bolsters the hypothesis of an early
441 occupation by *H. sapiens* before 40 ka, and supports ESR ages obtained from Middle
442 Paleolithic layers, which gives an age estimate for the onset of occupation in the cave, starting
443 from MIS 5.
444 From a methodological perspective, the low U-content in most of the dental tissues
445 allows to calculate EU-ESR ages without encountering the usual uncertainties resulting from
446 the reconstruction of the unknown U-uptake history. However, considering that the dose rates
447 in dental tissues are negligible and that the gamma doses are also low, the cosmic dose rate
448 represents up to 47% of the annual dose. Therefore, it was computed specifically for each
449 sample considering the morphology of the cave and the distance between each sample and the

entrance. This study highlighted two aspects of the application of ESR dating to Late Pleistocene karstic sites: 1) a large dependence on the gamma and cosmic dose rates for which variations may significantly affect the ages; and 2) the low uranium concentrations induce a negligible internal dose rate, thus allowing the calculation of meaningful and finite EU-ESR age results that are indistinguishable from the US-ESR estimates.

In the context of the end of the Middle Paleolithic, the study of Neanderthal occupations within a chronological framework at Geißenklösterle cave is fundamental to assess the spatiotemporal disappearance of this population from Europe, as well as to understand group dynamics during the Late Pleistocene. ESR ages obtained in this study suggest that groups of Neanderthals occasionally occupied the cave between MIS 5 and 4, from 94 ± 10 ka to 55 ± 6 ka, and provide for the first time chronological constraints for the base of the sequence.

Moreover, the presence of an almost sterile layer (GH 17), dated by ESR to 46 ± 3 ka (weighted mean age), could represent the end of human activities and the abandonment of the site. Taking into account that the ^{14}C ages for early Aurignacian deposits are older than Heinrich Stadial 4 by several thousands of years, we can conclude that *H. neanderthalensis* likely occupied the site until Heinrich Stadial 5, before the arrival of *H. sapiens* in the area. This raises questions about the relationship between these two species in this region. Did they really meet in the Swabian Jura? This is a core question, especially when we focus on the absence of transitional industries in this area, and the few human remains documented in the region. A complete chronological study of the Middle Palaeolithic sites of Swabian Jura needs to be carried out in the future, especially for major cave sites such as Hohle Fels, Sirgenstein, Kogelstein and Große Grotte to establish a well-defined chronological framework for the Swabian Middle Paleolithic.

Acknowledgments

This work was part of a Ph.D. dissertation funded by the French Ministry of Higher Education and Research, carried out at the MNHN. We thank S. Münzel, M. Malina and A. Janas (University of Tübingen), respectively for providing the teeth samples analyzed in this study, for the help in site comprehension and the assistance during fieldwork. We are grateful to O. Tombret and J.-J. Bahain (MNHN) for their help in the acquisition and the discussion of alpha and gamma spectrometry data. We thank E. Douville (LSCE) for providing access to ICP-QMS in LSCE and L. Bordier (LSCE) for performing the measurements. We thank the two anonymous reviewers for their constructive remarks on this manuscript.

References

Adamiec, G., Aitken, M.J., 1998. Dose-rate conversion factors: update. Ancient TL 16, 37-50.

Beck, J.W., Richards, D.A., Lawrence, R., Silverman, B.W., Smart, P.L., Donahue, D.J., Hererra-Osterheld, S., Burr, G.S., Calsoyas, L., Timothy, A., 2001. Extremely large variations of atmospheric ^{14}C concentration during the last glacial period. Science 292, 2453-2458.

Bischoff, J.L., Rosenbauer, R.J., Tavoso, A., de Lumley, H., 1988. A test of uranium-series dating of fossil tooth enamel: results from Tournal Cave, France. Applied Geochemistry 3, 145-151.

Brennan, B.J., Rink, W.J., McGuirl, E.L., Schwarcz, H.P., Prestwich, W.V., 1997. Beta doses in tooth enamel by “one-group” theory and the ROSY ESR dating software. Radiation Measurements 27, 307-314.

Bronk Ramsey, C., Lee, S., 2013. Recent and planned developments of the program OxCal. Radiocarbon 55, 720-730.

499 Conard, N., 2002. The timing of cultural innovations and the dispersal of modern humans in
500 Europe. Terra Nostra 6, 82-94.
501 Conard, N.J., 2003. Palaeolithic ivory sculptures from southwestern Germany and the origins
502 of figurative art. Nature 426, 830-832.
503 Conard, N.J., 2006. Changing views of the relationship between Neanderthals and modern
504 humans. In: Conard, N.J. (Ed.), When Neanderthals and Modern Humans Met. Kerns
505 Verlag, Tübingen, pp. 5-20.
506 Conard, N.J., 2009. A female figurine from the basal Aurignacian of Hohle Fels Cave in
507 southwestern Germany. Nature 459, 248-252.
508 Conard, N.J., 2010. Cultural modernity: Consensus or conundrum? Proceedings of the
509 National Academy of Sciences USA 107, 7621-7622.
510 Conard, N.J., 2011. The demise of the Neanderthal cultural niche and the beginning of the
511 Upper Paleolithic in Southwestern Germany. In: Conard, N.J., Richter, J. (Eds.),
512 Neanderthal Lifeways, Subsistence and Technology. Springer Netherlands, Dordrecht,
513 pp. 223-240.
514 Conard, N.J., 2015. Cultural Evolution During the Middle and Late Pleistocene in Africa and
515 Eurasia. In: Henke, W., Tattersall, I. (Eds.), Handbook of Paleoanthropology. Springer,
516 Berlin, pp. 2465-2508.
517 Conard, N.J., Bolus, M., 2003. Radiocarbon dating the appearance of modern humans and
518 timing of cultural innovations in Europe: new results and new challenges. Journal of
519 Human Evolution 44, 331-371.
520 Conard, N.J., Bolus, M., 2008. Radiocarbon dating the late Middle Paleolithic and the
521 Aurignacian of the Swabian Jura. Journal of Human Evolution 55, 886-897.

522 Conard, N.J., Bolus, M., Goldberg, P., Münzel, S.C., 2006. The last Neanderthals and first
523 modern humans in the Swabian Jura. In: Conard, N.J. (Ed.), When Neanderthals and
524 Modern Humans Met. Kerns Verlag, Tübingen, pp. 305-341.
525 Conard, N.J., Malina, M., Munzel, S.C., 2009. New flutes document the earliest musical
526 tradition in southwestern Germany. Nature 460, 737-740.
527 Conard, N.J., Bolus, M., Münzel, S.C., 2012. Middle Paleolithic land use, spatial organization
528 and settlement intensity in the Swabian Jura, southwestern Germany. Quaternary
529 International 247, 236-245.
530 d'Errico, F., 2003. The invisible frontier. A multiple species model for the origin of behavioral
531 modernity. Evolutionary Anthropology 12, 188-202.
532 d'Errico, F., Zilhao, J., Julien, L., Baffier, D., Pelegrin, J., 1998. Neanderthal acculturation in
533 Western Europe? Current Anthropology 39, S1-S44.
534 Douka, K., Higham, T.F.G., Wood, R., Boscato, P., Gambassini, P., Karkanas, P., Peresani,
535 M., Ronchitelli, A.M., 2014. On the chronology of the Uluzzian. Journal of Human
536 Evolution 68, 1-13.
537 Douville, E., Sallé, E., Frank, N., Eisele, M., Pons-Branchu, E., Ayrault, S., 2010. Rapid and
538 accurate U–Th dating of ancient carbonates using inductively coupled plasma-
539 quadrupole mass spectrometry. Chemical Geology 272, 1-11.
540 Duval, M., Grün, R., 2016. Are published ESR dose assessments on fossil tooth enamel
541 reliable? Quaternary Geochronology 31, 19-27.
542 Eggins, S., Grün, R., Pike, A.W.G., Shelley, M., Taylor, L., 2003. ^{238}U, ^{232}Th profiling and U-
543 series isotope analysis of fossil teeth by laser ablation-ICPMS. Quaternary Science
544 Reviews 22, 1373-1382.
545 Floss, H., 2017. Same as it ever was? The Aurignacian of the Swabian Jura and the origins of
546 Palaeolithic art. Quaternary International. https://doi.org/10.1016/j.quaint.2016.12.044

547 Grün, R., 2000. Methods of dose determination using ESR spectra of tooth enamel. Radiation
548 Measurements 32, 767-772.
549 Grün, R., 2009. The DATA program for the calculation of ESR age estimates on tooth
550 enamel. Quaternary Geochronology 4, 231-232.
551 Grün, R., Katzenberger-Apel, O., 1994. An alpha irradiator for ESR dating. Ancient TL 12,
552 35-38.
553 Grün, R., Schwarcz, H.P., Chadam, J., 1988. ESR dating of tooth enamel: Coupled correction
554 for U-uptake and U-series disequilibrium. International Journal of Radiation
555 Applications and Instrumentation. Part D. Nuclear Tracks and Radiation Measurements
556 14, 237-241.
557 Guthrie D. 1990. Frozen Fauna of the Mammoth Steppe. The Story of Blue Babe. University
558 of Chicago Press, London.
559 Hahn, J., 1971. La statuette masculine de la Grotte du Hohlenstein-Stadel (Wurtemberg).
560 L'Anthropologie 75, 233-244.
561 Hahn, J., 1982. Eine menschliche Halbreliefdarstellung aus der Geißenklösterle-Höhle bei
562 Blaubeuren. Fundberichte aus Baden-Württemberg 7, 1-12.
563 Hahn, J., 1988. Die Geißenklösterle-Höhle im Achtal bei Blaubeuren I. Fundhorizontbildung
564 und Besiedlung im Mittelpaläolithikum und im Aurignacien. Konrad Theiss Verlag,
565 Stuttgart.
566 Hahn, J., 1995. Neue Beschleuniger-^{14}C-Daten zum Jungpaläolithikum in
567 Südwestdeutschland. Eiszeitalter und Gegenwart 45, 86-92.
568 Harvati-Papatheodorou, K., 2013. Neanderthals. In: Begun, D.R. (Ed.), A Companion to
569 Paleoanthropology. Blackwell Publishing, Oxford, pp. 538-556.

570 Higham, T., 2011. European Middle and Upper Palaeolithic radiocarbon dates are often older
571 than they look: problems with previous dates and some remedies. Antiquity 85, 235-
572 249.
573 Higham, T., Brock, F., Peresani, M., Broglio, A., Wood, R., Douka, K., 2009. Problems with
574 radiocarbon dating the Middle to Upper Palaeolithic transition in Italy. Quaternary
575 Science Reviews 28, 1257-1267.
576 Higham, T., Compton, T., Stringer, C., Jacobi, R., Shapiro, B., Trinkaus, E., Chandler, B.,
577 Groning, F., Collins, C., Hillson, S., O'Higgins, P., FitzGerald, C., Fagan, M., 2011. The
578 earliest evidence for anatomically modern humans in northwestern Europe. Nature 479,
579 521-524.
580 Higham, T., Basell, L., Jacobi, R., Wood, R., Ramsey, C.B., Conard, N.J., 2012. Testing
581 models for the beginnings of the Aurignacian and the advent of figurative art and music:
582 the radiocarbon chronology of Geißenklösterle. Journal of Human Evolution 62, 664-
583 676.
584 Hockett, B., Haws, J.A., 2005. Nutritional ecology and the human demography of Neandertal
585 extinction. Quaternary International 137, 21-34.
586 Hofreiter, M., Münzel, S., Conard, N.J., Pollack, J., Slatkin, M., Weiss, G., Pääbo, S., 2007.
587 Sudden replacement of cave bear mitochondrial DNA in the late Pleistocene. Current
588 Biology 17, R122-R123.
589 Housley, R.A., Gamble, C.S., Street, M., Pettitt, P., 1997. Radiocarbon evidence for the late
590 glacial human recolonisation of Northern Europe. Proceedings of the Prehistoric Society
591 63, 25-54.
592 Hublin, J.-J., 2012. The earliest modern human colonization of Europe. Proceedings of the
593 National Academy of Sciences USA 109, 13471-13472.

Hublin, J.-J., Spoor, F., Braun, M., Zonneveld, F., Condemi, S., 1996. A late Neanderthal associated with Upper Palaeolithic artefacts. Nature 381, 224-226.

Ikeya, M., 1982. A model of linear uranium accumulation for ESR age of Heidelberg (Mauer) and Tautavel bones. Japanese Journal of Applied Physics 21, L690.

Kind, J.-C., Ebinger-Rist, N., Wolf, S.F., Beutelspacher, T., Wehrberger, K., 2014. The smile of the Lion Man. Recent excavations in Stadel Cave (Baden-Württemberg, south-western Germany) and the restoration of the famous Upper Palaeolithic figurine. Quartär 61, 129-145.

Kitagawa, H., van der Plicht, J., 1998. Atmospheric radiocarbon calibration to 45,000 yr BP: Late Glacial fluctuations and cosmogenic isotope production. Science 279, 1187-1190.

Kohn, M.J., 2008. Models of diffusion-limited uptake of trace elements in fossils and rates of fossilization. Geochimica et Cosmochimica Acta 72, 3758-3770.

Mallol, C., Hernández, C.M., Machado, J., 2012. The significance of stratigraphic discontinuities in Iberian Middle-to-Upper Palaeolithic transitional sites. Quaternary International 275, 4-13.

Mellars, P., 1999. The Neanderthal problem continued. Current Anthropology 40, 341-364.

Mellars, P., 2004. Neanderthals and the modern human colonization of Europe. Nature 432, 461-465.

Mellars, P., 2005. The impossible coincidence. A single-species model for the origins of modern human behavior in Europe. Evolutionary Anthropology 14, 12-27.

Miller, C.E., 2015. A Tale of Two Swabian Caves. Geoarchaeological investigations at Hohle Fels and Geißenklösterle. Kerns Verlag, Tübingen.

Müller, U.C., Pross, J., Tzedakis, P.C., Gamble, C., Kotthoff, U., Schmiedl, G., Wulf, S., Christanis, K., 2011. The role of climate in the spread of modern humans into Europe. Quaternary Science Reviews 30, 273-279.

619 Münzel, S.C., 2001. The production of Upper Palaeolithic mammoth bone artifacts from
620 southwestern Germany. In: Cavarretta, G., Gioia, P., Mussi, M., Palombo, M.R. (Eds.),
621 The World of Elephants. Consiglio Nazionale delle Ricerche, Roma, pp. 448-454.
622 Münzel, S.C., Conard, N.J., 2004. Change and continuity in subsistence during the Middle
623 and Upper Palaeolithic in the Ach Valley of Swabia (south-west Germany).
624 International Journal of Osteoarchaeology 14, 225-243.
625 Peresani, M., 2008. A new cultural frontier for the Last Neanderthals: The Uluzzian in
626 Northern Italy. Current Anthropology 49, 725-731.
627 Ponte, J.M., Font, E., Veiga-Pires, C., Hillaire-Marcel, C., Ghaleb, B., 2017. The effect of
628 speleothem surface slope on the remanent magnetic inclination. Journal of Geophysical
629 Research: Solid Earth 122, 4143-4156.
630 Prescott, J.R., Hutton, J.T., 1988. Cosmic ray and gamma ray dosimetry for TL and ESR.
631 International Journal of Radiation Applications and Instrumentation. Part D. Nuclear
632 Tracks and Radiation Measurements 14, 223-227.
633 Rasmussen, S.O., Bigler, M., Blockley, S.P., Blunier, T., Buchardt, S.L., Clausen, H.B.,
634 Cvijanovic, I., Dahl-Jensen, D., Johnsen, S.J., Fischer, H., Gkinis, V., Guillevic, M.,
635 Hoek, W.Z., Lowe, J.J., Pedro, J.B., Popp, T., Seierstad, I.K., Steffensen, J.P.,
636 Svensson, A.M., Vallelonga, P., Vinther, B.M., Walker, M.J.C., Wheatley, J.J.,
637 Winstrup, M., 2014. A stratigraphic framework for abrupt climatic changes during the
638 Last Glacial period based on three synchronized Greenland ice-core records: refining
639 and extending the INTIMATE event stratigraphy. Quaternary Science Reviews 106, 14-
640 28.
641 Reimer, P.J., Bard, E., Bayliss, A., Beck, J.W., Blackwell, P.G., Bronk Ramsey, C., Buck,
642 C.E., Cheng, H., Edwards, R.L., Friedrich, M., Grootes, P.M., Guilderson, T.P.,
643 Haflidason, H., Hajdas, I., Hatté, C., Heaton, T.J., Hoffmann, D.L., Hogg, A.G.,

644 Hughen, K.A., Kaiser, K.F., Kromer, B., Manning, S.W., Niu, M., Reimer, R.W.,
645 Richards, D.A., Scott, E.M., Southon, J.R., Staff, R.A., Turney, C.S.M., van der Plicht,
646 J., 2013. IntCal13 and Marine13 Radiocarbon Age Calibration Curves 0–50,000 Years
647 cal BP. Radiocarbon 55, 1869-1887.
648 Richard, M., Falguères, C., Pons-Branchu, E., Bahain, J.J., Voinchet, P., Lebon, M., Valladas,
649 H., Dolo, J.M., Puaud, S., Rué, M., Daujeard, C., Moncel, M.H., Raynal, J.P., 2015.
650 Contribution of ESR/U-series dating to the chronology of late Middle Palaeolithic sites
651 in the middle Rhône valley, southeastern France. Quaternary Geochronology 30, 529-
652 534.
653 Richard, M., Falguères, C., Pons-Branchu, E., Ghaleb, B., Valladas, H., Mercier, N., Richter,
654 D., Bahain, J.-J., Conard, N.J., 2017. Datation par les méthodes ESR/U-Th combinées
655 de sites du Pléistocène supérieur : méthodologie et application en contexte karstique.
656 L'Anthropologie 121, 63-72.
657 Richter, D., 2007. Advantages and limitations of thermoluminescence dating of heated flint
658 from Paleolithic sites. Geoarchaeology 22, 671-683.
659 Richter, D., Waiblinger, J., Rink, W.J., Wagner, G.A., 2000. Thermoluminescence, electron
660 spin resonance and ^{14}C-dating of the late Middle and early Upper Palaeolithic site of
661 Geißenklösterle Cave in Southern Germany. Journal of Archaeological Science 27, 71-
662 89.
663 Richter, D., Tostevin, G., Škrdla, P., Davies, W., 2009. New radiometric ages for the Early
664 Upper Palaeolithic type locality of Brno-Bohunice (Czech Republic): comparison of
665 OSL, IRSL, TL and ^{14}C dating results. Journal of Archaeological Science 36, 708-720.
666 Sauvet, G., Fritz, C., Tosello, G., 2008. Emergence et expansion de l'art aurignacien. Bulletin
667 de la Société Préhistorique Ariège-Pyrénées 63, 33-46.

668 Seierstad, I.K., Abbott, P.M., Bigler, M., Blunier, T., Bourne, A.J., Brook, E., Buchardt, S.L.,
669 Buizert, C., Clausen, H.B., Cook, E., Dahl-Jensen, D., Davies, S.M., Guillevic, M.,
670 Johnsen, S.J., Pedersen, D.S., Popp, T.J., Rasmussen, S.O., Severinghaus, J.P.,
671 Svensson, A., Vinther, B.M., 2014. Consistently dated records from the Greenland
672 GRIP, GISP2 and NGRIP ice cores for the past 104 ka reveal regional millennial-scale
673 $\delta^{18}O$ gradients with possible Heinrich event imprint. Quaternary Science Reviews 106,
674 29-46.
675 Svensson, A., Andersen, K.K., Bigler, M., Clausen, H.B., Dahl-Jensen, D., Davies, S.M.,
676 Johnsen, S.J., Muscheler, R., Parrenin, F., Rasmussen, S.O., Röthlisberger, R.,
677 Seierstad, I., Steffensen, J.P., Vinther, B.M., 2008. A 60 000 year Greenland
678 stratigraphic ice core chronology. Climate of the Past 4, 47-57.
679 Villa, P., Roebroeks, W., 2014. Neandertal demise: an archaeological analysis of the modern
680 human superiority complex. PLoS One 9, e96424.
681 Verpoorte, A., 2006. Neanderthal energetics and spatial behaviour. Before Farming 2006, 1-6.
682 Voelker, A.H., Grootes, P.M., Nadeau, M.-J., Sarnthein, M., 2000. Radiocarbon levels in the
683 Iceland Sea from 25–53 kyr and their link to the Earth's magnetic field intensity.
684 Radiocarbon 42, 437-452.
685 White, R., 1982. Rethinking the Middle/Upper Paleolithic Transition. Current Anthropology
686 23, 85-108.
687 Wood, R.E., Barroso-Ruíz, C., Caparrós, M., Jordá Pardo, J.F., Galván Santos, B., Higham,
688 T.F.G., 2013. Radiocarbon dating casts doubt on the late chronology of the Middle to
689 Upper Palaeolithic transition in southern Iberia. Proceedings of the National Academy
690 of Sciences USA 110, 2781-2786.
691 Yokoyama, Y., Falguères, C., Quaegebeur, J.P., 1985. ESR dating of quartz from quaternary
692 sediments: First attempt. Nuclear Tracks and Radiation Measurements 10, 921-928.

693 Zilhão, J., d'Errico, F., Bordes, J.-G., Lenoble, A., Texier, J.-P., Rigaud, J.-P., 2006. Analysis
694 of Aurignacian interstratification at the Châtelperronian-type site and implications for
695 the behavioral modernity of Neandertals. Proceedings of the National Academy of
696 Sciences USA 103, 12643-12648.
697

698 **Figure captions**

699

700 **Figure 1.** Location of Geißenklösterle (red dot) and other Late Pleistocene sites (black dot) in
701 the Ach and Lone Valleys, Swabian Jura (Baden-Württemberg, Germany). Redrawn from
702 Figure 19.1. in Conard (2011).

703

704 **Figure 2.** Stratigraphic column, teeth locations (white stars) and weighted mean ages obtained
705 at Geißenklösterle. M: Magdalenian; G: Gravettian; UA: upper Aurignacian; LA: lower
706 Aurignacian; OH: occupational hiatus; MP: Middle Palaeolithic. Redrawn from profile E
707 from Figure 40 in Miller (2015).

708

709 **Figure 3.** Lithic artifacts from early Aurignacian layers. Reproduced from Hahn (1988).

710

711 **Figure 4.** Lithic artifacts from Late Middle Paleolithic layers. 1, 2: sidescrapers; 3: retouched
712 flake with faceted platform remnant. Reproduced from Conard et al. (2006).

713

714 **Figure 5.** Map of Geißenklösterle (top right) with measured (red) and assumed (blue) roof
715 thickness and photographs of the sections showing both dosimeters and sediment samples
716 locations.

717

718 **Figure 6.** Cross section of the cave and 3D cosmic dose modelling. The cosmic dose field can
719 be modelled as a cone with an angle of 30° in relation to the vertical axis, providing around
720 65% of the cosmic dose rate, while cones with angles between 30° and 60° and 60° and 90°
721 provide around 30% and 5% of the cosmic dose rate, respectively. Translated from Figure 5 in
722 Richard et al. (2017).
723
724 **Figure 7.** ESR dose response curves of samples GK 76-1080, GH 15 (a) and GK 47-583, GH
725 21 (b).
726
727 **Figure 8.** Relative contributions of alpha, beta, gamma and cosmic dose rates (%) to the total
728 dose rate calculated for the ages presented in Table 5.
729
730 **Figure 9.** Graphical representation of ages as a function of the depth and the $\delta^{18}O$ variations
731 (North Greenland Ice Core Project (NGRIP) dataset (Rasmussen et al., 2014; Seierstad et al.,
732 2014), available on www.iceandclimate.dk/data).
733
734 **Figure 10.** Comparison of published ^{14}C, TL and ESR ages (1σ) with ESR ages obtained in
735 this study. ^{14}C ages are calibrated using IntCal13 (Reimer et al., 2013) and Oxcal 4.2 (Bronk
736 Ramsey and Lee, 2013).

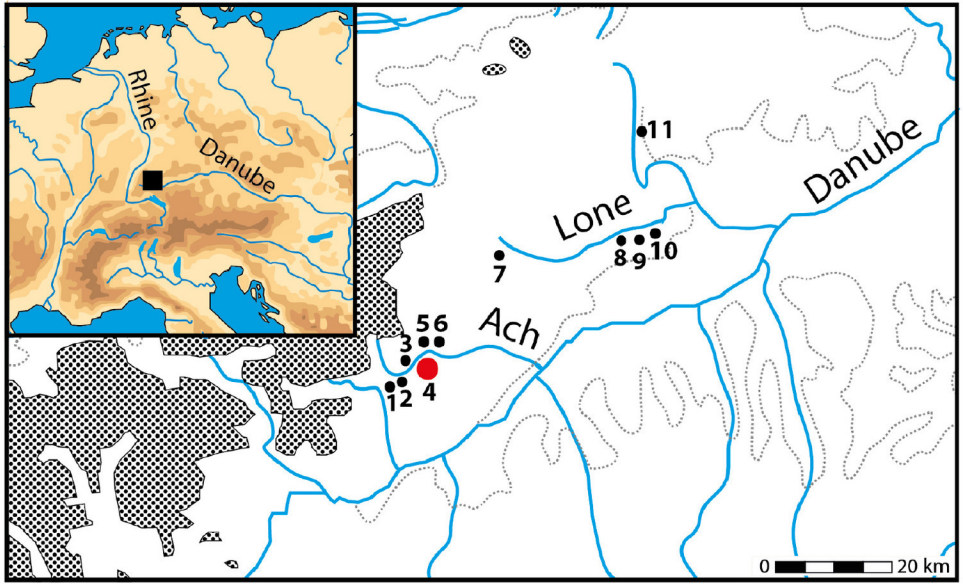

1 : Kogelstein
2 : Hohle Fels
3 : Sirgenstein
4 : Geißenklösterle
5 : Brillenhöhle
6 : Große Grotte
7 : Haldenstein
8 : Bockenstein
(Bockstein-Höhle,
Bocksteinloch,
Bocksteinschmiede
and Bockstein-Törle)
9 : Hohlenstein
(Stadel and Bärenhöhle)
10 : Vogelherd
11 : Heidenschmiede

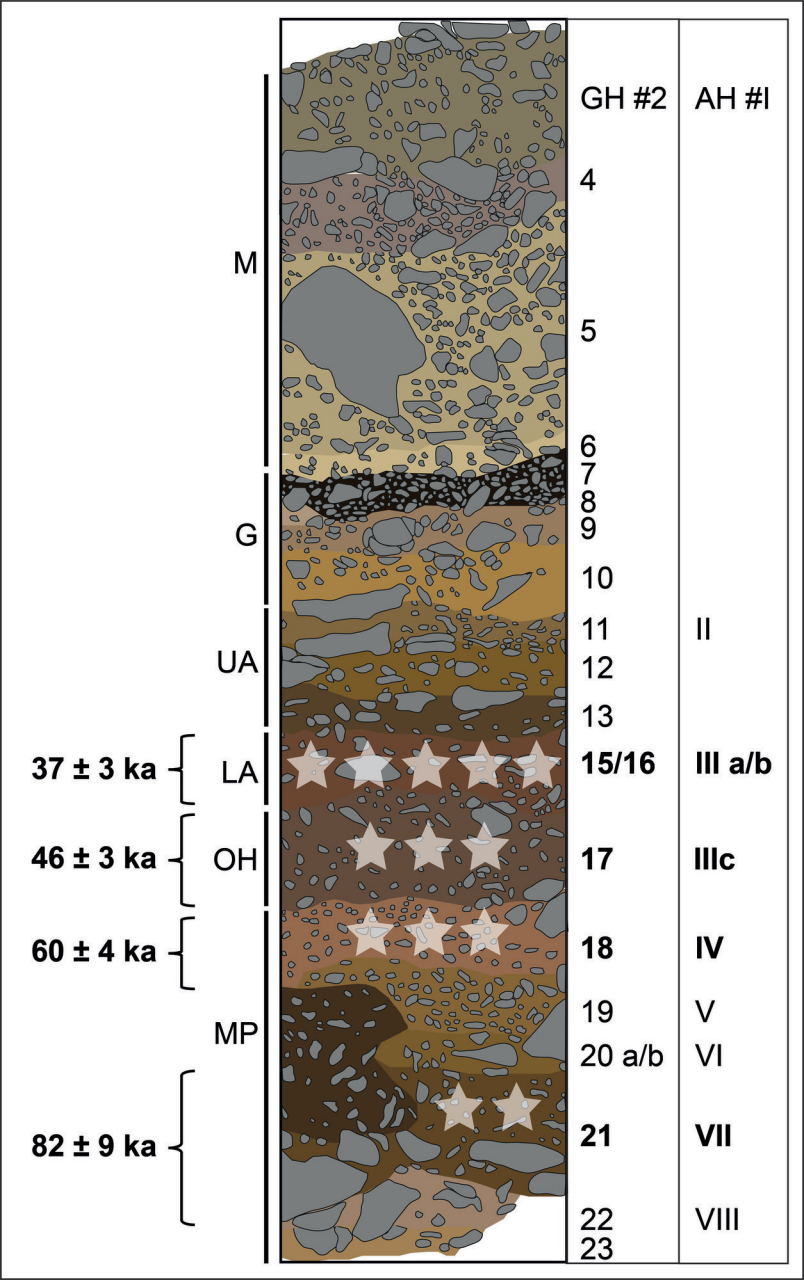
GH #2
AH #I
M
4
5
6
7
8
G
9
10
UA
11
II
12
13
37 ± 3 ka
LA
15/16
III a/b
46 ± 3 ka
OH
17
IIIc
60 ± 4 ka
18
IV
MP
19
V
20 a/b
VI
82 ± 9 ka
21
VII
22
VIII
23


1
2
3
0
5 cm

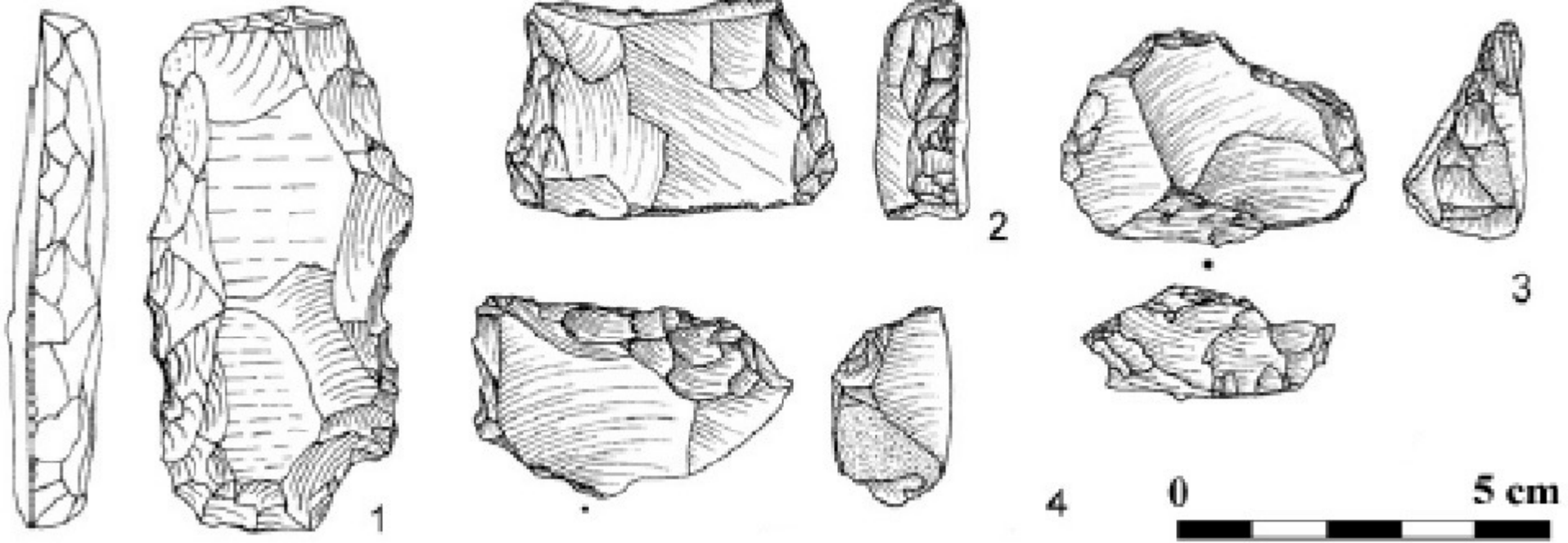
1
2
3
4
0
5 cm

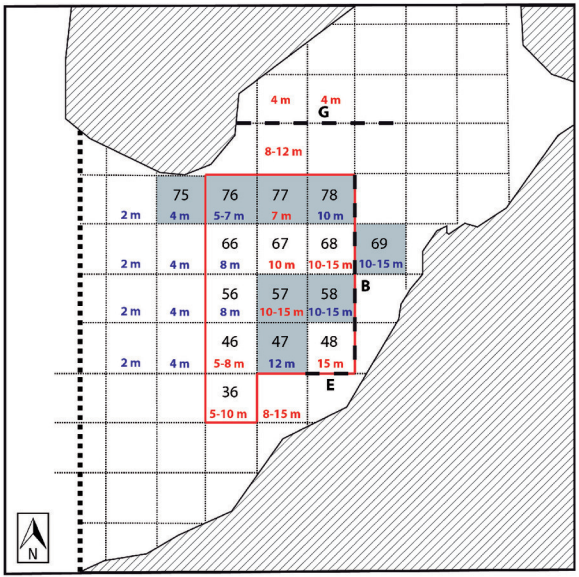

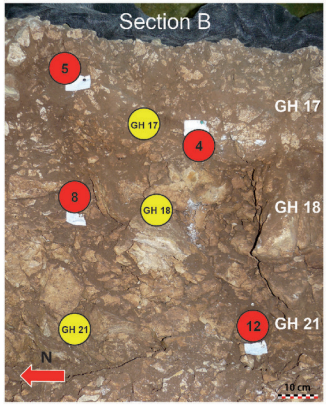

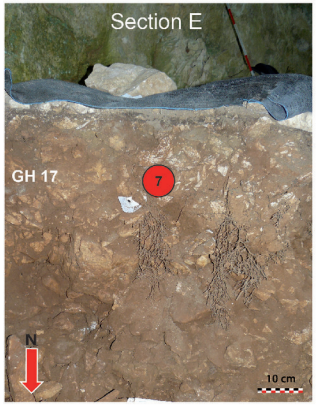

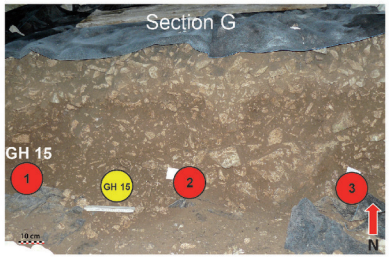

Dosimeter

Sediment sample

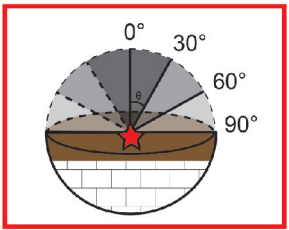
0°
30°
60°
90°
θ

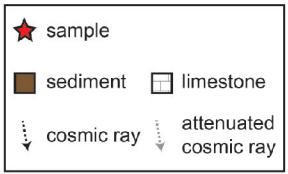
sample
sediment
limestone
cosmic ray
attenuated cosmic ray

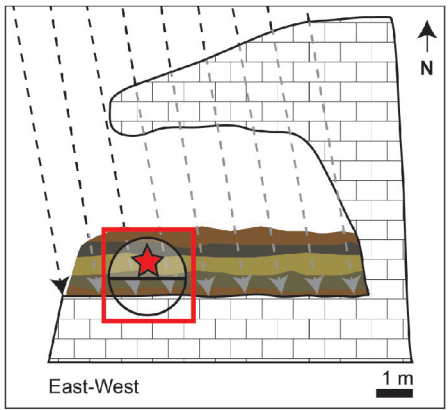
N
East-West
1 m

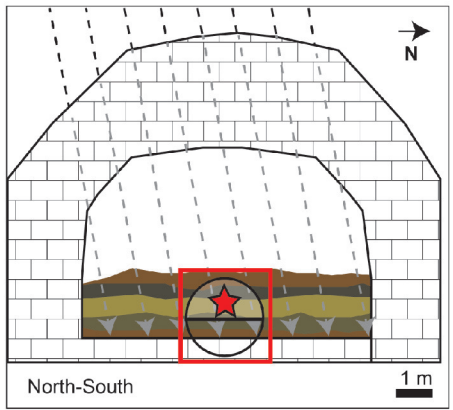
N
North-South
1 m

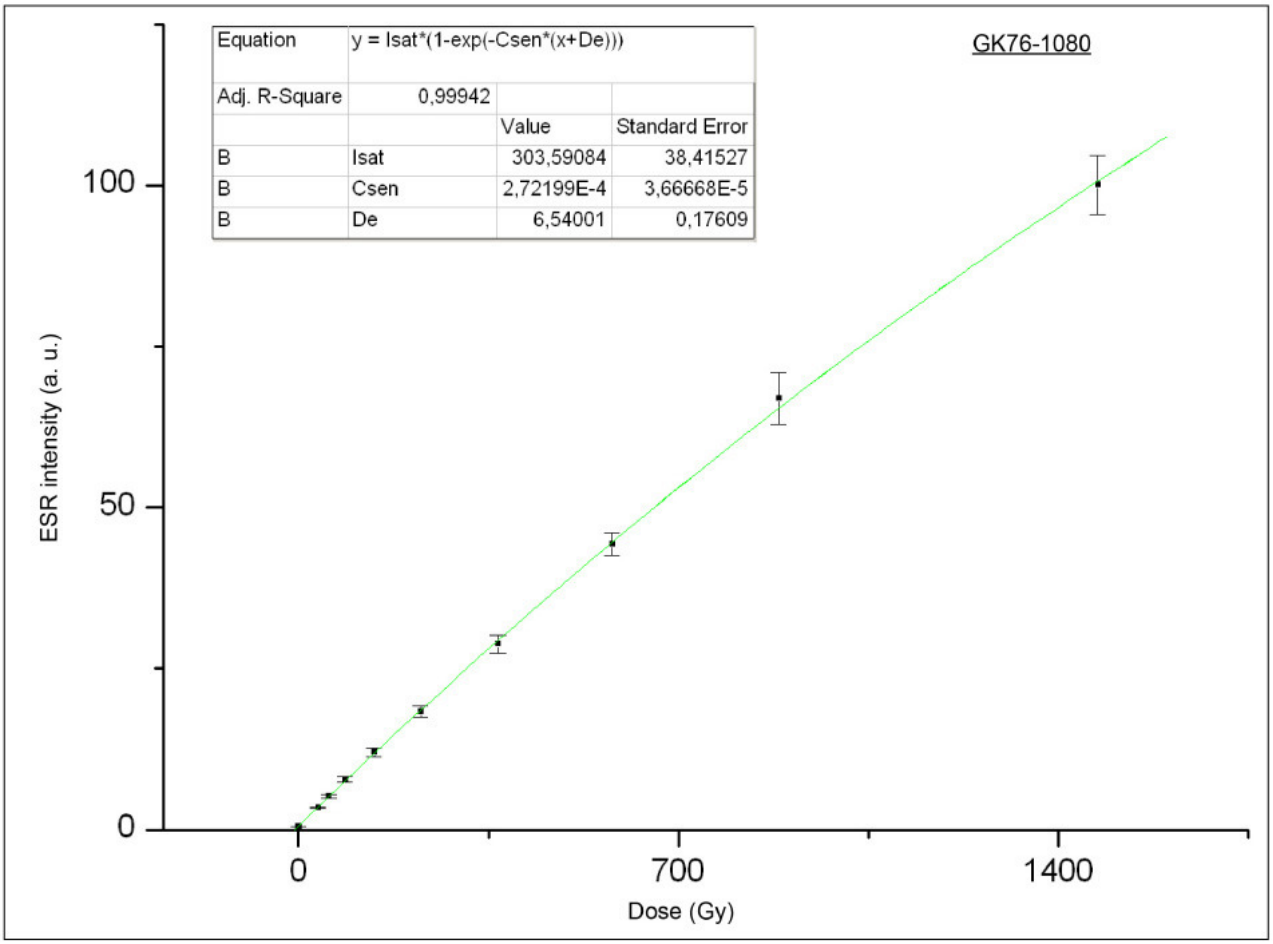
Equation
y = Isat*(1-exp(-Csen*(x+De)))
Adj. R-Square
0,99942
Value
Standard Error
B
Isat
303,59084
38,41527
B
Csen
2,72199E-4
3,66668E-5
B
De
6,54001
0,17609
GK76-1080
ESR intensity (a. u.)
100
50
0
0
700
1400
Dose (Gy)

a)

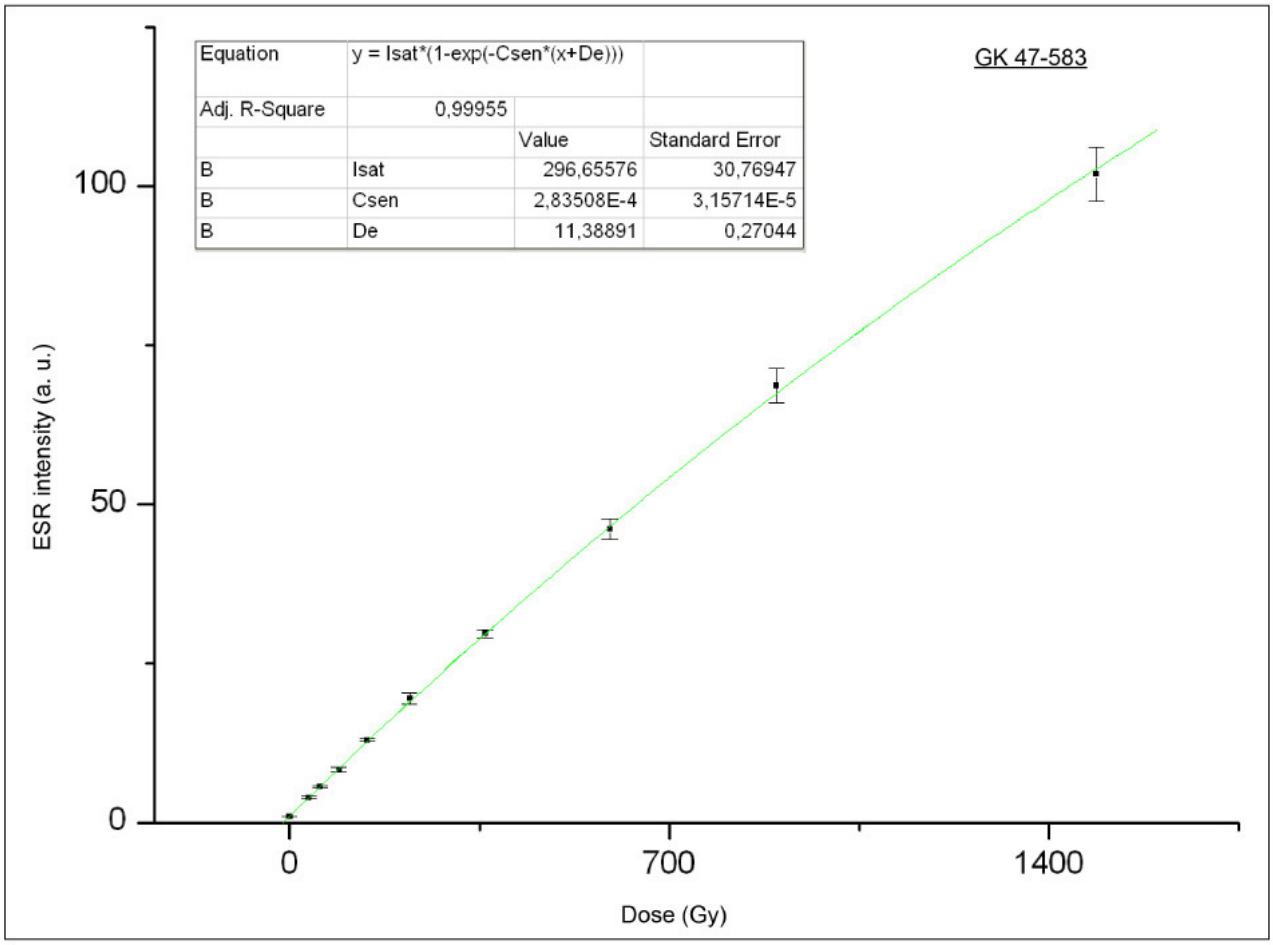
Equation
y = Isat*(1-exp(-Csen*(x+De)))
Adj. R-Square
0,99955
Value
Standard Error
B
Isat
296,65576
30,76947
B
Csen
2,83508E-4
3,15714E-5
B
De
11,38891
0,27044
GK 47-583
ESR intensity (a. u.)
100
50
0
0
700
1400
Dose (Gy)

b)

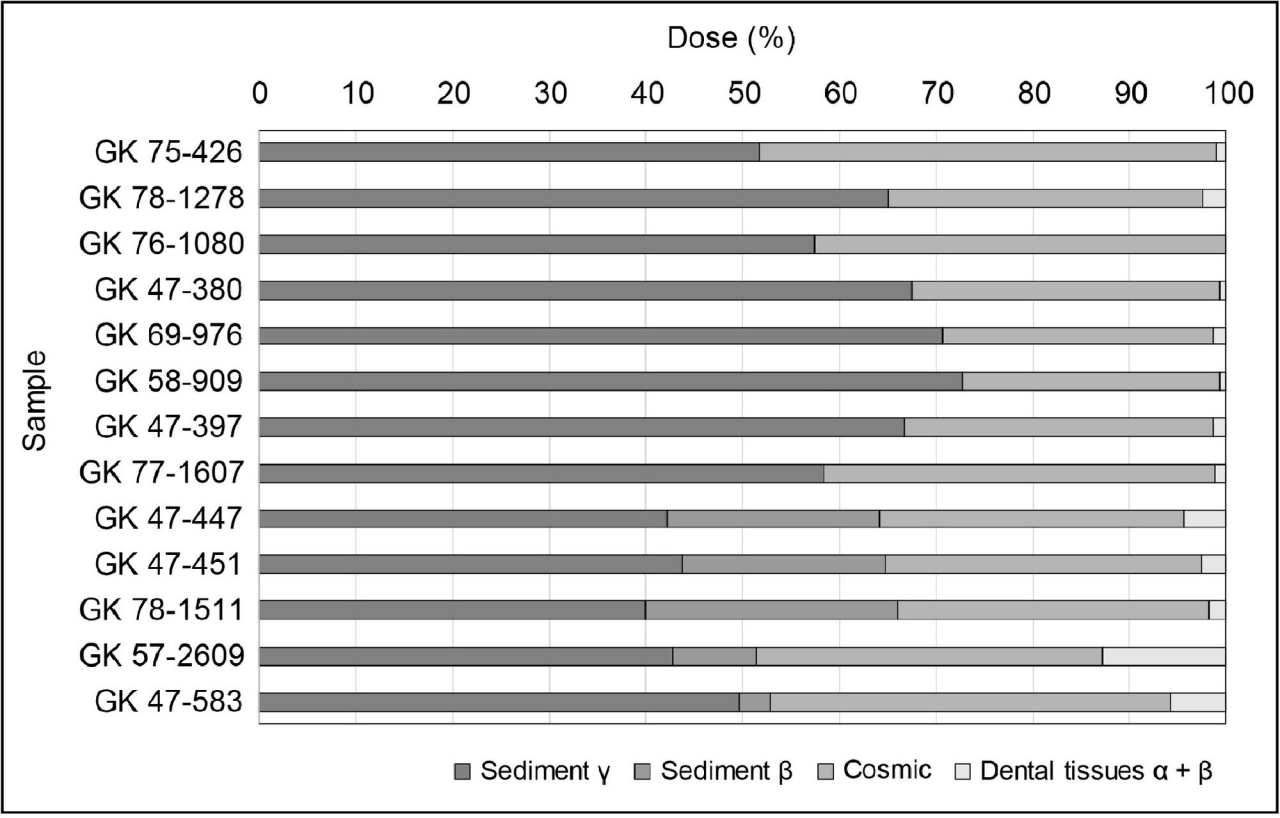
Dose (%)
0
10
20
30
40
50
60
70
80
90
100
Sample
GK 75-426
GK 78-1278
GK 76-1080
GK 47-380
GK 69-976
GK 58-909
GK 47-397
GK 77-1607
GK 47-447
GK 47-451
GK 78-1511
GK 57-2609
GK 47-583
Sediment γ
Sediment β
Cosmic
Dental tissues α + β

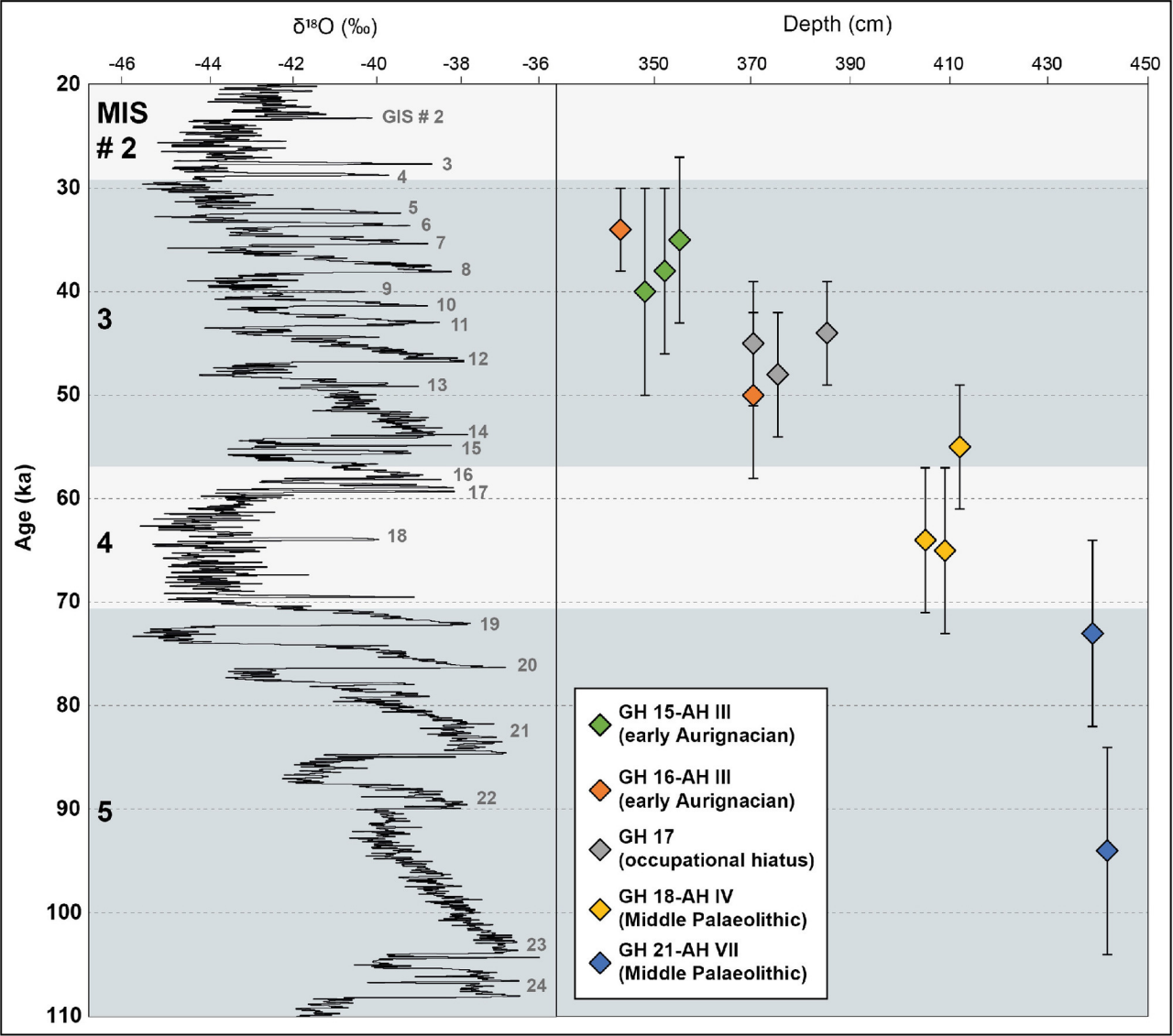
δ18O (‰)
-46
-44
-42
-40
-38
-36
Depth (cm)
350
370
390
410
430
450
Age (ka)
20
30
40
50
60
70
80
90
100
110
MIS
2
3
4
5
GIS # 2
3
4
5
6
7
8
9
10
11
12
13
14
15
16
17
18
19
20
21
22
23
24
GH 15-AH III
(early Aurignacian)
GH 16-AH III
(early Aurignacian)
GH 17
(occupational hiatus)
GH 18-AH IV
(Middle Palaeolithic)
GH 21-AH VII
(Middle Palaeolithic)

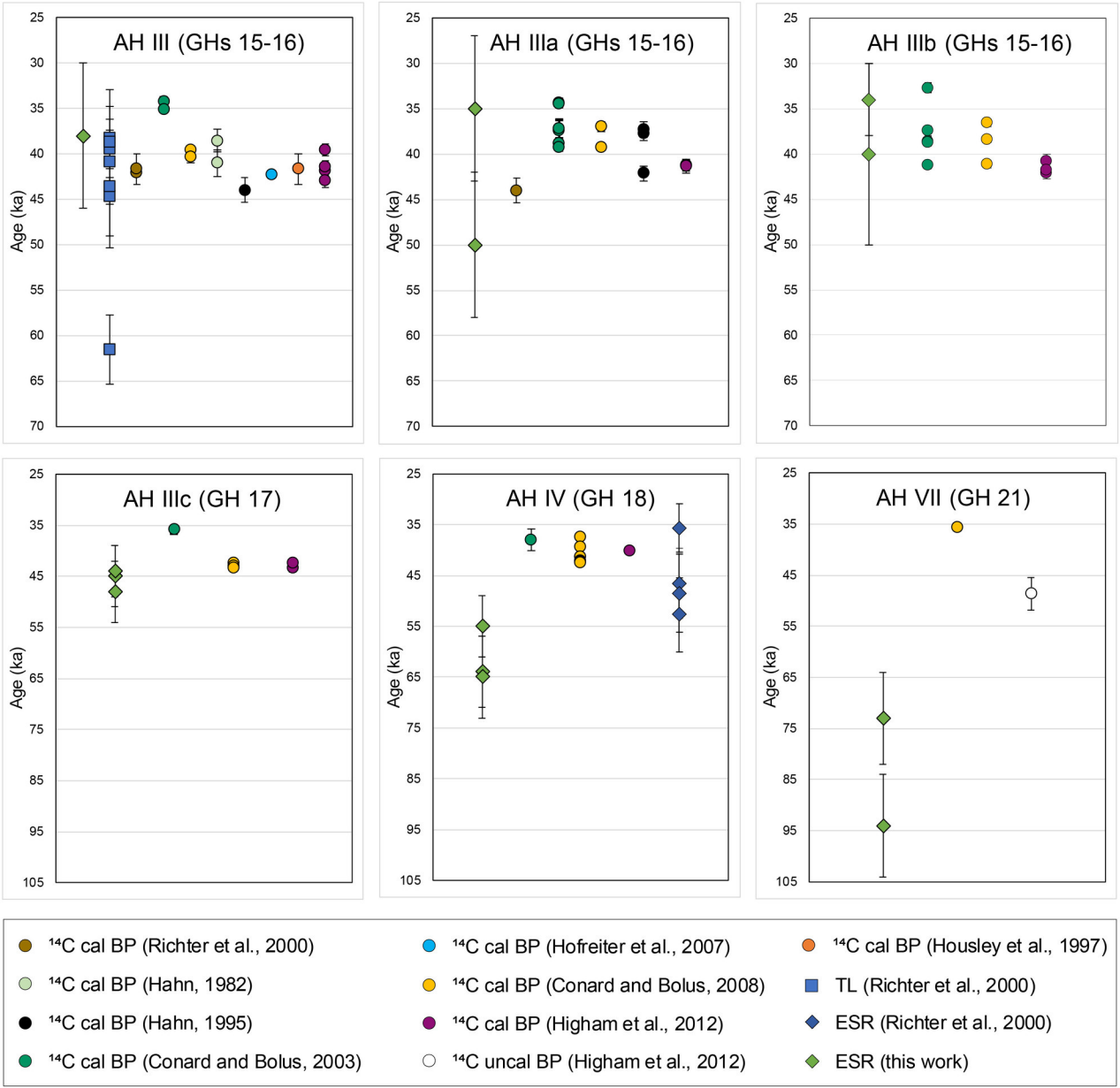
AH III (GHs 15-16)
AH IIIa (GHs 15-16)
AH IIIb (GHs 15-16)
AH IIIc (GH 17)
AH IV (GH 18)
AH VII (GH 21)
Age (ka)
25
30
35
40
45
50
55
60
65
70
75
85
95
105
14C cal BP (Richter et al., 2000)
14C cal BP (Hofreiter et al., 2007)
14C cal BP (Housley et al., 1997)
14C cal BP (Hahn, 1982)
14C cal BP (Conard and Bolus, 2008)
TL (Richter et al., 2000)
14C cal BP (Hahn, 1995)
14C cal BP (Higham et al., 2012)
ESR (Richter et al., 2000)
14C cal BP (Conard and Bolus, 2003)
14C uncal BP (Higham et al., 2012)
ESR (this work)

Table 1

Sample type, laboratory number, geological (GH) and archaeological (AH) horizons, coordinates and taxonomic determination of samples from Geißenklösterle. The map and grid of the cave are available in Figure 5.

Type	Lab N°	GH	AH	Square	X (m)	Y (m)	Z (m)	Taxon	Grain size (µm)[a]
Tooth	GK 75-426	15	III	75	25.57	29.13	-3.52	*Equus* sp.	100–200
Tooth	GK 78-1278	15	IIIb	78	28.49	29.85	-3.48	*Equus* sp.	100–200
Tooth	GK 76-1080	15	IIIa	76	26.59	29.72	-3.55	*Equus* sp.	0–200
Sediment	GK.sed.GH15	15	III	99	29.21	31.12	-3.30	—	—
Tooth	GK 47-380	16	IIIa	47	27.41	26.66	-3.70	*Equus* sp.	100–200
Tooth	GK 69-976	16	IIIb	69	29.83	28.72	-3.43	*Equus* sp.	100–200
Tooth	GK 58-909	17	IIIc	58	28.19	27.85	-3.70	*Equus* sp.	100–200
Tooth	GK 47-397	17	IIIc	47	27.42	26.57	-3.75	*Equus* sp.	100–200
Tooth	GK 77-1607	17	IIIc	77	27.05	29.06	-3.85	*Equus* sp.	100200
Sediment	GK.sed.GH17	17	IIIc	69	29.17	28.37	-3.82	—	—
Tooth	GK 47-447	18	IV	47	27.06	26.96	-4.12	*Capra ibex*	0–200
Tooth	GK 47-451	18	IV	47	27.44	26.43	-4.05	*Capra ibex*	100–200
Tooth	GK 78-1511	18	IV	78	28.50	29.05	-4.09	*Capra ibex*	0–200
Sediment	GK.sed.GH18	18	IV	69	29.16	28.28	-4.13	—	—
Tooth	GK 57-2609	21	VII	57	27.13	27.96	-4.39	*Equus* sp.	0–200
Tooth	GK 47-583	21	VII	47	27.83	26.20	-4.42	*Rhinoceros* sp.	100–200
Sediment	GK.sed.GH21	21	VII	69	29.19	28.63	-4.57	—	—

[a] ESR analyses are commonly carried out on the 100–200 µm granulometric fraction and U-Th on the 0–100 µm fraction. For powder samples weighing less than 500 mg, the 0–100 and 100-200 µm granulometric fractions were combined and ESR measurements were performed before U-Th analysis.

Table 2

U-Th data (U-content and isotopic ratios) and initial and removed thickness on side 1 (dentine) and side 2 (cement or sediment).

Sample	GH	Tissue	[^{238}U] (ppm)	^{234}U/^{238}U	^{230}Th/^{234}U	Enamel (initial thickness, µm)	Side 1 (removed thickness, µm)	Side 2 (removed thickness, µm)
GK 75-426	15	E	0.0024 ± 0.0001	nd	nd	1201 ± 120	88 ± 9	67 ± 7
		D	0.0213 ± 0.0001	1.0872 ± 0.0242	0.8249 ± 0.2152			
		C	0.2336 ± 0.0013	1.2043 ± 0.0057	0.1111 ± 0.0080			
GK 78-1278	15	E	0.0027 ± 0.0001	1.3579 ± 0.0418	nd	1177 ± 118	128 ± 13	54 ± 5
		D	0.1040 ± 0.0006	1.3526 ± 0.0231	0.6644 ± 0.0171			
		C	0.3650 ± 0.0025	1.1613 ± 0.0130	0.1246 ± 0.0037			
GK 76-1080	15	E	0.0041 ± 0.0001	1.5452 ± 0.0570	nd	1137 ± 114	99 ± 10	169 ± 17
		D[a]	0.0314 ± 0.022	nd	nd			
		C	0.0492 ± 0.0004	1.1855 ± 0.0481	0.3468 ± 0.0201			
GK 47-380	16	E	0.0033 ± 0.0001	1.3840 ± 0.3685	nd	1190 ± 119	106 ± 11	105 ± 11
		D[a]	0.0346 ± 0.0143	nd	nd			
		C[a]	0.1617 ± 0.0213	nd	nd			
GK 69-976	16	E	0.0037 ± 0.0001	1.6266 ± 0.4542	nd	1161 ± 116	119 ± 12	61 ± 6
		D[a]	0.0376 ± 0.0155	nd	nd			
		C[a]	0.1797 ± 0.0327	nd	nd			
GK 58-909	17	E	0.0033 ± 0.0001	1.4217 ± 0.3458	nd	1374 ± 137	77 ± 8	74 ± 7
		D	0.0120 ± 0.0001	1.3358 ± 0.0274	nd			
		C	0.0969 ± 0.0007	1.2396 ± 0.0134	0.1231 ± 0.0068			
GK 47-397	17	E	0.0026 ± 0.0001	1.6419 ± 0.7889	nd	1238 ± 124	117 ± 12	77 ± 8
		D	0.0319 ± 0.0002	1.2473 ± 0.0277	0.4596 ± 0.0462			
		C	0.2904 ± 0.0018	1.2474 ± 0.0201	0.1915 ± 0.0055			
GK 77-1607	17	E	0.0082 ± 0.0001	1.4501 ± 0.0149	nd	1288 ± 129	116 ± 12	22 ± 2
		D	0.0984 ± 0.0014	1.2987 ± 0.1183	0.1750 ± 0.0285			
		C	0.0364 ± 0.0002	nd	nd			
GK 47-447	18	E	0.0294 ± 0.0001	1.2475 ± 0.0207	0.2614 ± 0.0291	821 ± 82	37 ± 4	25 ± 3
		D	0.0627 ± 0.0004	1.2751 ± 0.0102	0.3601 ± 0.0168			
GK 47-451	18	E	0.0108 ± 0.0001	1.8344 ± 0.3333	nd	847 ± 45	78 ± 8	67 ± 7
		D	0.0390 ± 0.0002	1.2282 ± 0.0611	0.1971 ± 0.0203			
GK 78-1511	18	E	0.0106 ± 0.0001	1.2740 ± 0.0410	nd	698 ± 70	149 ± 15	31 ± 3
		D	0.0541 ± 0.0003	1.2413 ± 0.0637	0.2113 ± 0.0098			
GK 57-2609	21	E	0.2583 ± 0.0016	1.3632 ± 0.0124	0.2018 ± 0.0079	1057 ± 106	211 ± 21	24 ± 2
		D	0.0556 ± 0.0001	1.2319 ± 0.0342	0.1272 ± 0.0074			
GK 47-583	21	E	0.0264 ± 0.0001	1.3225 ± 0.0590	nd	2346 ± 235	87 ± 9	95 ± 9

	D	0.0664 ± 0.0005	1.3057 ± 0.0185	0.2460 ± 0.0123

Abbreviations: nd = not detectable; E = enamel; D = dentine; C = cement; GH = geological horizon.

[a] These samples were analysed using alpha spectrometry according to a chemical procedure detailed in Bischoff et al. (1988).

Table 3

^{238}U, ^{232}Th and ^{40}K measured using a HPGe gamma spectrometer. The position of each sediment sample is available in Figure 5.

Sample	GH	^{238}U (ppm)	^{232}Th (ppm)	^{40}K (%)
GK.sed.GH15	15	0.94 ± 0.07	2.89 ± 0.10	0.30 ± 0.01
GK.sed.GH17	17	0.54 ± 0.07	2.37 ± 0.01	0.22 ± 0.01
GK.sed.GH18	18	0.58 ± 0.07	1.59 ± 0.09	0.16 ± 0.01
GK.sed.GH21	21	0.20 ± 0.05	0.81 ± 0.06	0.06 ± 0.01

Abbreviation: GH = geological horizon.

Table 4

In situ gamma dosimetry. Dosimeter number and associated section, coordinates and dose rate (see map of the cave and photographs of the section in Fig. 5).

GH	No.	Section	x (m)	y (m)	z (m)	γ dose rate (µGy/a)	Mean value (µGy/a)
15	1	G	28.789	31.122	-3.30	145	108 ± 42
15	2	G	29.632	31.086	-3.34	66	
15	3	G	30.434	31.047	-3.34	113	
16	—	—	—	—	—	—	106 ± 23[a]
17	4	B	29.168	28.173	-3.92	88	104 ± 18
17	5	B	29.182	28.62	-3.68	103	
17	7	E	28.477	26.413	-3.79	122	
18	8	B	29.184	28.587	-4.08	67	67 ± 17[b]
21	12	B	29.134	27.977	-4.48	60	60 ± 15[b]

Abbreviation: GH = geological horizon.

[a] This value corresponds to a mean value obtained from measurements in both GHs 15 and 17 (see text).

[b] A 20% error range was estimated for these values, from gamma dose variations observed in GHs 15 and 17.

Table 5

Equivalent doses, dose rates and EU-ESR or US-ESR (bold) ages.

Sample	GH	D_e (Gy)	Dose rate (μGy/a)					Age (ka)
			Sediment (γ)	(β)	Cosmic[a]	Tooth (α + β)	Total (α + β + γ)	
GK 75-426	15	7.92 ± 0.24	108 ± 42	—	99 ± 10	2 ± 1	209 ± 41	38 ± 8
GK 78-1278		6.63 ± 0.16	108 ± 42	—	54 ± 5	4 ± 1	166 ± 40	40 ± 10
GK 76-1080		6.54 ± 0.18	108 ± 42	—	80 ± 8	—	188 ± 40	35 ± 8
GK 47-380	16	7.75 ± 0.31	106 ± 23	—	50 ± 5	1 ± 1	157 ± 22	50 ± 8
GK 69-976		4.94 ± 0.18	106 ± 23	—	42 ± 4	2 ± 2	150 ± 22	34 ± 4
GK 58-909	17	6.42 ± 0.29	104 ± 18	—	38 ± 4	1 ± 1	143 ± 18	45 ± 6
GK 47-397		7.56 ± 0.20	104 ± 18	—	50 ± 5	2 ± 1	156 ± 18	48 ± 6
GK 77-1607		7.87 ± 0.23	104 ± 18	—	72 ± 7	2 ± 1	178 ± 19	44 ± 5
GK 47-447	18	8.69 ± 0.24	67 ± 17	35 ± 4	50 ± 5	7 ± 1	159 ± 15	55 ± 6
GK 47-451		9.74 ± 0.24	67 ± 17	32 ± 4	50 ± 5	4 ± 2	153 ± 15	64 ± 7
GK 78-1511		10.92 ± 0.36	67 ± 17	44 ± 6	54 ± 5	3 ± 1	168 ± 15	65 ± 8
GK 57-2609	21	10.15 ± 0.46	60 ± 15	12 ± 2	50 ± 5	18 ± 5	140 ± 14	**73 ± 9**[b]
GK 47-583		11.39 ± 0.27	60 ± 15	4 ± 1	50 ± 5	7 ± 1	121 ± 13	94 ± 10

Abbreviation: GH = geological horizon.

[a] A 10% error was estimated for the cosmic dose.

[b] US-ESR age with associated *p*-values of 0.80 ± 0.40 (enamel) and 2.15 ± 0.17 (dentine).